Received: 30 May 2022 | Accepted: 31 August 2022

DOI: 10.1111/arcm.12825

ORIGINAL ARTICLE

Reflections into Ptolemaic glass: Colorless, white, blue, and green inlays from the workshop of Tebtynis

Cinzia Bettineschi[1,2] | **Ivana Angelini**[2]

[1]Department of Classical Archaeology, University of Augsburg, Augsburg, Germany

[2]Department of Cultural Heritage: Archaeology and History of Art, Cinema and Music, University of Padua, Padua, Italy

Correspondence
Cinzia Bettineschi, Department of Cultural Heritage: Archaeology and History of Art, Cinema and Music, University of Padua, Capitaniato Square 7, 35139 Padua, Italy.
Email: cinzia.bettineschi@philhist.uni-augsburg.de and cinzia.bettineschi@unipd.it

Funding information
Analyses were funded by the University of Padua among the most innovative research proposed by students (proposing PhD student: CB; reference professor: IA) in the framework of project "ArExGlass: Archaeometry and Experimental Archaeology for Pre-Roman Glassworking" (2017–2018).

Abstract

Inlays range among the most aesthetically pleasing and technically challenging glasses produced in the Ptolemaic period. Despite the central role of this phase in the history of glass technology, little is known about the recipes and the technological knowledge of the Egyptian artisans. This paper will thus focus on the study of the materials from the secondary workshop of Tebtynis (Fayum oasis, Egypt). We report the first multi-methodological study comprising textural, chemical, and mineralogical analyses (optical microscopy, scanning electron microscopy coupled with energy-dispersive system, electron probe microanalysis, and μ-Raman spectroscopy) on a set of 81 colorless, white, blue, and green samples carefully selected among the 800+ glasses from the craft area now stored at the Museo Egizio, Turin (Italy).

Our study offers the biggest compositional database of well-dated Ptolemaic glasses currently available in the literature, highlighting some interesting novelties regarding the silica and alkali sources, and the coloring and opacifying techniques employed. The results suggest a specialized craft of traditional origin, but open to innovation and experimentation, as expected from transitional phases.

KEYWORDS

Egyptian archaeology, glass inlays, mineral phases, Ptolemaic period, raw materials, secondary workshop

INTRODUCTION

Archaeological glass has long been considered a privileged means to explore multiple aspects of past societies, from ideology and belief to economy, trade, and consumption, from social structure to technological evolution and organization of the production, from the use and functionality of the artifacts to waste management and recycle.

Nowadays, it is generally accepted that Egypt had a central role in the early history of glass, being the only place where a number of glass workshops ranging from the 2nd millennium BCE to the 1st millennium CE were discovered and excavated (Nenna, 2015; Nicholson, 2007; Push & Rehren, 2007).

Shortland and Eremin (2006) noted that "the study of Egyptian glass represents the most important window on the origins of man-made glass". However, while the contexts and the artifacts of the Late Bronze Age (Egyptian New Kingdom) were investigated in detail by various authors, our knowledge on the composition of the glass dated to the Late and the Ptolemaic periods (approx. 7th to early 1st century BCE) is generally limited—so much that the 1st millennium BCE was recently defined as "the dark age" of Egyptian glass (Rehren & Rosenow, 2020). Nevertheless, the Ptolemaic period is a transitional moment of crucial importance in the evolution of glassmaking, as it set the basis for the revolution of glass blowing, which took place around the last quarter of the 1st century BCE (on this subject see, among others, Grose, 1989; Stern, 2012). Moreover, it is a key phase for Egypt in setting up the large-scale production and export of glass that led to its widespread trade throughout the Mediterranean in the late Republican and early Imperial era.

This work is thus focused on the archaeometric study of a collection of more than 800 fragments of monochrome and polychrome glasses discovered by the Italian Archaeological Mission in Egypt (MAI) in the inlay workshop of Tebtynis (Fayum oasis, Figure 1) in 1931 and currently preserved at the Museo Egizio, Turin (Italy). The Tebtynis workshop stands as a landmark in vitreous materials studies, not only because it yielded a huge quantity of semi-finished and finished products, but mostly because it preserved the tools, the kiln, and the room furniture which were used for glassmaking (Bettineschi, Deotto, et al., 2019).

Even though all the archaeological documentation regarding the location of the workshop and the planimetry of the structures was never published at the end of the excavations, the site is widely cited in the literature among the few Hellenistic glass-working centers known in the Mediterranean basin (see, e.g., Henderson, 2013; Larson, 2016; Nenna et al., 2000; Stern & Schlick-Nolte, 1994). Recently, study of the archives of Carlo Anti, director of the Tebtynis excavations, offered the chance to obtain first-hand data on the discovery of the workshop and its materials (Bettineschi, Deotto, et al., 2019). The research revealed that the workshop of Tebtynis was located within the first court of the Soknebtynis temple, that it was abandoned in correspondence with a functional transformation of the area, and that the glass inlays recovered and brought back to Italy constitute a reference assemblage, selected to offer a statistically significant overview of all the materials unearthed.

MATERIALS AND METHODS

The Museo Egizio (ME) of Turin preserves more than 800 fragments of vitreous materials from Tebtynis bigger than ~2 mm. The number of micro-chips, often in mosaic glass, is significantly higher. Most of the collection is constituted by finished, semi-finished, and waste fragments of inlays in opaque and transparent glass, suggesting a uniform original context (the workshop), eventually complemented by its products discovered among the sanctuary and the town.

The first step of the work was devoted to sorting the inlays into meaningful groups. Using a classification based on their technological complexity, the collection includes: (a) monochrome

FIGURE 1 Localization of Tebtynis in the framework of Graeco-Roman inlay workshops in Egypt (Bettineschi, Angelini, & Molin, 2019)

inlays; (b) stratified inlays; and (c) figured inlays in mosaic glass. Monochrome glasses can be divided into two main categories: simple bars/rods and figurative elements representing clothes, furniture, or parts of the human body. Stratified glasses usually have from two up to seven layers of alternating colors, while mosaic canes and slices represent a huge variety of motifs, generally connected to the Egyptian iconography: rosettes and lotus flowers, *ankh-was* hieroglyphs, stars, and other mixed designs.

The assemblage shows a wide range of colored, opaque glasses: from red, brown, orange, and yellow to blue, light blue, green, and white. Translucent and transparent glasses are also present, sometimes in the classic pale green of non-intentionally colored glass. Preliminary stereo microscopy (SM) observations allowed us to group the glasses into seven main classes considering their color, hue, opacity, homogeneity, and texture. These classes comprise: one type of opaque brown; one of opaque white; two types of transparent colorless glass (true colorless and aqua); two of opaque red (dull red and sealing-wax red); one of opaque yellow and one yellowish-orange; two of green (transparent green and opaque turquoise) and three of blue (transparent and opaque dark blue, and opaque light blue). One additional violet-blue class was attributed to weathering processes, and all other small variations to possible differences in the quantity and quality of coloring, decoloring, and opacifying agents.

A total of 70 objects, with 144 different glass types, were selected for in-depth archaeometric investigations (see Supporting Information, Table S1). Due to the quantity and complexity of the results obtained, in this work we present the data related to the colorless, white, blue, and green samples, which constitute the majority of the analyzed specimens.

The analytical protocol was designed to guarantee the complete characterization of the samples and the cross-validation of the data. The instruments used include SM, optical microscopy (OM), scanning electron microscopy coupled with energy-dispersive system (SEM-EDS), electron probe microanalysis (EPMA), and μ-Raman spectroscopy. A detailed discussion of the techniques and software employed, as well as the experimental conditions, can be found in the supplementary materials (Supporting Information, Experimental and Tables S2 and S3).

RESULTS

Silica source

The chemical composition of the amorphous phase of the analyzed samples is summarized in Table 1. EPMA data show that all samples are soda-lime silica and lead silica glasses with SiO_2 ranging from 43.81% to 73.19%, where the lowest silica values can be attributed to leaded glasses. The use of sand as the main silica source in all the analyzed samples is testified by the high quantity of both Al_2O_3, ranging from 0.91% to 2.95% (average 2.17%) and FeO, in the range of 0.28–2.52% (average 1.29%). FeO ≤ 0.5% is found especially in colorless, white, light blue, and turquoise samples, suggesting that purified or purer sand was probably selected for this kind of glass; in any case, the corresponding alumina is high, from 1.81% to 2.39%, so the use of crushed quartzite or quartz-rich pebbles should be discarded.

Considering the plot FeO versus TiO_2 (Figure 2a), there is a clear positive trend that can be interpreted as a combined contribution from the sand (Turner, 1956).

From the textural point of view, SEM-EDS highlighted the presence of various crystalline inclusions related to unreacted relics of the original raw materials or impurities introduced during the glass-forming/assembly in a sand-rich environment. The most common inclusion identified is quartz (μ-Raman data), which is present in all the main color classes—except colorless glasses—in varying sizes (from a few microns up to 150 μm) and mainly rounded. Other widespread sand-related light minerals include epidotes, pyroxenes, and feldspars (both alkali and plagioclase feldspars). Fe and especially Fe-Ti oxides (frequently in an ilmenite-type stoichiometry with traces of Mg or Mn) are also regularly present in almost all glass colors. Corundum was identified in three samples: the greatest occurrence (120–150 μm with respect to an average of 10–20 μm) was found in S-TA-005-A and is characterized by inclusions of Ti-Fe/Fe oxides.

Flux composition

The alkali content is extremely variable: excluding altered samples, Na_2O ranges from 12.55% to 18.29%, K_2O from 0.32% to 2.12%, CaO from 2.03% to 9.99%, and MgO from 0.35% to 5.16%. The low Na_2O values in four samples can be attributed to a heavy or moderate weathering of the glass, as supported by SEM–backscattered electron (BSE) images. These samples were not considered for further statistical analyses. Lead, which can also act as a fluxing agent, is present in different concentrations, from as low as under the detection limit to as high as 24.19 wt%.

In general terms, this wide compositional range shows that different glass recipes were used. The plot K_2O versus MgO (Figure 2b), classically used to discriminate the type of alkali used, shows that most of the samples lay in the compositional range of low-magnesium glasses (LMG), produced using natron as fluxing agent (Henderson, 1985; Jackson et al., 2018). Within the natron group, K_2O ranges from 0.32% to 1.20%, MgO from 0.35% to 1.48%, and Na_2O from 8.67% to 18.29%. Minor elements, such as P, S, and Cl, also agree with the values typical of this compositional class. A uniform group of five white glasses clusters for its high MgO (4.98–5.16%) content, associated with a very low K_2O, of the order of 0.52–0.69%.

TABLE 1 EPMA results (glass phase). Chemical composition of the amorphous phase of the analyzed samples expressed as oxide weight percent and calculated as a mean of 5–7 point analyses

Sample name	Color		Na_2O	MgO	Al_2O_3	SiO_2	SO_3	P_2O_5	Cl	K_2O	CaO
I-B-616	Opaque dark blue	Mean	18.29	0.85	2.26	66.84	0.40	0.06	1.13	0.48	5.57
		SD	0.20	0.02	0.03	0.29	0.05	0.01	0.04	0.01	0.03
I-BBi-613-bi	Opaque white	Mean	13.20	1.48	2.15	59.65	0.80	0.43	0.38	1.29	5.49
		SD	0.08	0.04	0.08	0.06	0.02	0.04	0.04	0.03	0.17
I-BBi-613-BT	Transparent dark blue	Mean	17.65	0.64	2.23	70.26	0.04	0.42	1.01	0.89	5.72
		SD	0.26	0.04	0.08	0.26	0.03	0.03	0.02	0.06	0.07
M-A-005	Opaque light blue	Mean	17.26	0.79	2.49	65.51	0.08	0.20	1.53	0.54	7.24
		SD	0.34	0.07	0.06	0.21	0.02	0.02	0.03	0.02	0.17
M-A-005a	Opaque light blue	Mean	17.11	1.10	2.30	65.00	0.18	0.47	1.27	0.69	5.39
		SD	0.33	0.05	0.02	0.59	0.06	0.05	0.03	0.03	0.03
M-A-006	Opaque turquoise	Mean	13.47	0.52	0.91	67.20	0.05	0.31	0.98	0.32	2.03
		SD	0.17	0.04	0.04	0.54	0.04	0.10	0.03	0.02	0.06
M-B-002	Opaque dark blue	Mean	11.56	0.92	1.99	59.41	0.09	0.33	0.73	0.79	6.65
		SD	0.25	0.05	0.04	0.27	0.05	0.04	0.01	0.02	0.10
M-B-004	Transparent dark blue	Mean	14.55	0.44	2.08	71.30	0.05	0.31	1.30	0.58	5.30
		SD	0.39	0.01	0.02	0.44	0.02	0.02	0.04	0.02	0.05
M-BAu-002	Opaque dark blue	Mean	13.79	0.49	2.40	68.82	0.12	0.47	0.33	0.77	7.45
		SD	0.23	0.01	0.07	1.04	0.04	0.01	0.04	0.02	0.10
M-T-503	Aqua	Mean	15.93	2.59	2.25	66.29	0.20	0.92	0.94	1.60	6.95
		SD	0.89	0.66	0.04	1.98	0.06	0.14	0.03	0.02	0.04
M-T-503a	Aqua	Mean	15.23	1.70	2.12	67.75	0.24	0.71	0.97	1.64	6.51
		SD	0.01	0.09	0.05	0.11	0.04	0.03	0.04	0.01	0.09
M-V-005	Opaque turquoise	Mean	10.59	0.51	1.95	59.88	0.08	0.42	0.38	0.68	7.04
		SD	0.11	0.02	0.07	1.42	0.03	0.02	0.03	0.03	0.35

TABLE 1 (Continued)

Sample name	Color		Na_2O	MgO	Al_2O_3	SiO_2	SO_3	P_2O_5	Cl	K_2O	CaO
M-V-005a	Opaque turquoise	Mean	13.42	1.27	2.20	60.02	0.37	0.46	0.48	0.94	
		SD	0.47	0.03	0.03	0.43	0.06	0.05	0.04	0.03	0.23
M-V-006	Opaque turquoise	Mean	14.40	0.80	2.39	64.91	0.53	0.12	0.41	0.89	7.91
		SD	0.15	0.02	0.05	0.16	0.04	0.01	0.04	0.02	0.16
M-V-006a	Opaque turquoise	Mean	13.89	0.53	0.92	67.08	0.03	0.31	0.95	0.33	2.01
		SD	0.15	0.03	0.02	0.62	0.03	0.10	0.03	0.03	0.05
P-A-402-B	Opaque dark blue	Mean	13.76	0.48	2.59	67.10	0.39	0.07	0.32	0.85	7.29
		SD	0.19	0.01	0.04	0.22	0.01	0.03	0.10	0.06	0.15
P-A-408-B	Opaque dark blue	Mean	16.34	0.63	1.94	67.74	0.39	0.08	1.22	0.70	4.80
		SD	0.28	0.04	0.04	0.82	0.07	0.03	0.07	0.02	0.14
P-A-418-bi	Opaque white	Mean	16.37	2.61	2.69	65.37	0.06	0.30	0.99	0.71	7.98
		SD	0.30	0.05	0.05	0.80	0.02	0.02	0.02	0.02	0.07
P-A-418-BO	Opaque dark blue	Mean	14.62	0.60	2.49	67.44	0.19	0.24	0.92	0.72	6.43
		SD	0.26	0.01	0.06	0.18	0.04	0.02	0.04	0.01	0.04
P-A-419-bi	Opaque white	Mean	11.49	0.61	2.57	67.24	0.04	0.26	0.48	0.97	3.91
		SD	0.22	0.04	0.06	0.06	0.03	0.06	0.02	0.20	0.04
P-A-419-BT	Transparent dark blue	Mean	14.27	0.68	2.01	69.85	0.18	0.19	1.11	1.07	4.83
		SD	0.19	0.05	0.04	0.13	0.03	0.04	0.03	0.03	0.05
P-CR-421-A	Opaque light blue	Mean	15.76	0.45	2.08	69.55	0.07	0.31	1.76	0.47	4.95
		SD	0.01	0.03	0.03	0.73	0.02	0.04	0.06	0.02	0.20
P-CR-421-B	Opaque dark blue	Mean	15.30	0.69	2.68	69.07	0.12	0.23	1.06	0.70	6.31
		SD	0.12	0.03	0.04	0.30	0.03	0.05	0.03	0.01	0.06
P-CR-421-bi	Opaque white	Mean	0.13	0.42	2.05	75.73	0.04	0.41	1.13	0.43	5.30
		SD	0.01	0.01	0.05	0.77	0.01	0.02	0.05	0.02	0.07

TABLE 1 (Continued)

Sample name	Color		Na_2O	MgO	Al_2O_3	SiO_2	SO_3	P_2O_5	Cl	K_2O	CaO
P-CR-421-BT	Transparent dark blue	Mean	14.29	0.49	2.17	71.63	0.06	0.33	1.40	1.07	
		SD	0.42	0.03	0.04	0.31	0.04	0.09	0.05	0.03	0.04
P-FL-004-B	Opaque dark blue	Mean	16.27	0.71	2.77	68.77	0.10	0.19	1.21	0.85	5.22
		SD	0.17	0.03	0.03	0.13	0.02	0.04	0.06	0.01	0.03
P-FL-004-bi	Opaque white	Mean	16.54	5.04	1.96	67.73	0.04	0.24	0.87	0.69	6.25
		SD	0.13	0.05	0.02	0.24	0.04	0.05	0.02	0.11	0.06
P-FL-501-bi	Opaque white	Mean	12.66	0.51	2.40	70.36	0.04	0.47	0.64	1.20	3.48
		SD	0.34	0.02	0.04	0.13	0.03	0.17	0.08	0.07	0.09
P-FL-501-BT	Transparent dark blue	Mean	14.36	2.53	1.90	67.64	1.24	0.16	1.01	1.96	6.32
		SD	0.19	0.13	0.05	0.57	0.01	0.06	0.03	0.03	0.06
P-FR-422-B	Opaque dark blue	Mean	15.43	0.58	2.20	68.77	0.06	0.35	1.38	0.69	4.46
		SD	0.30	0.09	0.12	0.22	0.03	0.06	0.06	0.02	0.07
P-FR-422-bi	Opaque white	Mean	16.73	5.16	2.00	67.23	0.05	0.28	0.86	0.59	6.19
		SD	0.23	0.10	0.02	0.27	0.04	0.01	0.02	0.01	0.03
P-FR-422-T1	True colorless	Mean	15.99	0.52	2.22	71.22	0.04	0.32	1.41	0.73	5.53
		SD	0.11	0.02	0.04	0.33	0.02	0.06	0.05	0.03	0.02
Pn-B-001	Transparent dark blue	Mean	7.03	0.31	0.80	74.49	0.07	0.56	0.51	0.80	1.09
		SD	1.33	0.03	0.09	1.57	0.01	0.04	0.10	0.04	0.03
Pn-T-001	Aqua	Mean	17.92	0.92	2.35	66.90	0.31	0.23	1.04	0.97	6.08
		SD	1.78	0.07	0.12	4.30	0.05	0.06	0.02	0.04	0.26
P-R-414-BO	Opaque dark blue	Mean	17.07	0.73	2.87	68.43	0.12	0.24	1.19	0.88	5.22
		SD	0.45	0.03	0.05	0.20	0.03	0.02	0.04	0.01	0.08
P-R-414-T	True colorless	Mean	16.98	0.53	2.09	70.76	0.04	0.31	1.34	0.66	7.18
		SD	0.21	0.01	0.06	0.41	0.02	0.05	0.02	0.01	0.02

TABLE 1 (Continued)

Sample name	Color		Na_2O	MgO	Al_2O_3	SiO_2	SO_3	P_2O_5	Cl	K_2O	CaO
P-R-419-BO	Opaque dark blue	Mean	16.42	0.68	2.74	64.28	0.09	0.24	1.19	0.90	
		SD	0.28	0.03	0.08	0.87	0.03	0.03	0.05	0.03	0.03
P-R-419-BT	Transparent dark blue	Mean	17.30	0.47	2.15	69.17	0.05	0.28	1.43	0.66	5.42
		SD	0.52	0.02	0.01	0.49	0.02	0.04	0.04	0.05	0.02
P-R-419-VT	Transparent green	Mean	12.31	1.78	2.95	44.90	0.62	0.25	0.45	0.76	7.34
		SD	0.11	0.03	0.08	0.15	0.04	0.04	0.04	0.03	0.05
P-R-423-BO	Opaque dark blue	Mean	16.49	0.67	2.63	67.88	0.12	0.23	1.18	1.15	5.15
		SD	0.32	0.03	0.07	0.43	0.03	0.06	0.06	0.07	0.06
P-R-423-BT	Transparent dark blue	Mean	16.92	0.94	2.60	65.19	0.11	0.18	1.53	0.56	9.16
		SD	0.18	0.03	0.04	0.65	0.03	0.02	0.01	0.01	0.06
P-R-423-VT	Transparent green	Mean	17.19	4.19	2.44	62.52	1.74	0.34	1.15	2.12	8.51
		SD	0.23	0.02	0.04	0.59	0.02	0.01	0.05	0.03	0.06
P-St-415-B	Opaque dark blue	Mean	14.76	0.62	1.77	69.21	0.05	0.28	1.27	0.68	3.67
		SD	0.67	0.01	0.03	0.47	0.03	0.05	0.07	0.05	0.14
P-St-415-bi	Opaque white	Mean	11.43	0.52	2.48	70.34	0.07	0.27	0.62	0.93	3.63
		SD	0.61	0.03	0.12	0.21	0.04	0.04	0.01	0.03	0.16
P-StB-002	Opaque dark blue	Mean	13.22	0.89	2.51	66.46	0.19	0.43	0.46	0.90	7.37
		SD	0.17	0.01	0.03	0.42	0.04	0.02	0.02	0.02	0.09
P–T-417-bi	Opaque white	Mean	14.90	0.62	2.47	69.93	0.07	0.26	0.82	1.77	4.46
		SD	0.63	0.09	0.16	0.42	0.02	0.01	0.05	0.01	0.12
P–T-417-BO	Opaque dark blue	Mean	14.85	0.72	2.19	64.88	0.10	0.42	0.88	1.01	5.36
		SD	0.02	0.02	0.07	0.91	0.03	0.19	0.08	0.02	0.25
P–T-417-VT	Transparent green	Mean	16.89	4.61	1.02	60.67	1.73	0.24	0.97	1.81	9.99
		SD	0.35	0.02	0.03	0.40	0.05	0.05	0.01	0.06	0.01

TABLE 1 (Continued)

Sample name	Color		Na_2O	MgO	Al_2O_3	SiO_2	SO_3	P_2O_5	Cl	K_2O	CaO
S-423a-A	Opaque light blue	Mean	13.56	0.41	1.81	68.06	0.40	0.05	1.55	0.86	
		SD	0.42	0.04	0.05	0.89	0.03	0.03	0.04	0.02	0.08
S-423a-bi	Opaque white	Mean	16.26	4.98	1.85	66.98	0.33	0.03	0.80	0.60	6.23
		SD	0.24	0.03	0.01	0.51	0.05	0.02	0.01	0.09	0.02
S-423a-T	True colorless	Mean	15.06	0.47	2.07	69.97	0.38	0.04	1.35	0.82	5.24
		SD	0.19	0.01	0.05	0.19	0.03	0.01	0.01	0.02	0.06
S-ARG-403-A	Opaque light blue	Mean	15.55	0.48	2.20	69.00	0.07	0.30	1.56	0.49	4.72
		SD	0.18	0.02	0.05	0.34	0.01	0.04	0.01	0.01	0.07
Sb-B-003	Transparent dark blue	Mean	13.18	0.66	2.11	71.55	0.23	0.09	0.80	0.66	8.40
		SD	0.17	0.05	0.06	0.20	0.01	0.01	0.02	0.00	0.01
S-BB-004-BO	Opaque dark blue	Mean	15.54	0.69	2.60	67.89	0.09	0.19	1.19	0.87	5.21
		SD	0.17	0.02	0.08	0.48	0.04	0.05	0.03	0.02	0.03
S-BB-004-BT	Transparent dark blue	Mean	13.65	0.53	2.13	69.98	0.06	0.35	1.68	0.66	6.09
		SD	0.38	0.03	0.05	0.29	0.05	0.04	0.01	0.03	0.05
S-BBi-004-bi	Opaque white	Mean	14.34	0.60	1.65	71.57	0.07	0.31	0.89	0.71	3.82
		SD	0.73	0.03	0.06	3.19	0.03	0.06	0.05	0.07	0.48
S-BBi-004-BT	Transparent dark blue	Mean	16.53	0.54	1.61	71.34	0.02	0.25	1.32	0.41	4.29
		SD	1.00	0.12	0.08	2.50	0.01	0.16	0.13	0.14	0.30
S-BBi-004-BTc	Transparent dark blue	Mean	17.71	0.78	1.77	68.49	0.05	0.38	1.17	0.58	4.75
		SD	0.58	0.02	0.07	0.29	0.01	0.05	0.03	0.01	0.06
S-BBi-004-BTs	Transparent dark blue	Mean	16.01	0.50	1.66	73.19	0.04	0.17	1.43	0.38	4.26
		SD	0.10	0.04	0.04	0.17	0.00	0.02	0.03	0.05	0.06
S-BiBR-404-bi	Opaque white	Mean	16.98	5.05	1.99	66.77	0.04	0.28	0.85	0.56	6.25
		SD	0.21	0.03	0.03	0.27	0.03	0.06	0.03	0.04	0.03

TABLE 1 (Continued)

Sample name	Color		Na_2O	MgO	Al_2O_3	SiO_2	SO_3	P_2O_5	Cl	K_2O	CaO
S-BiBR-404-BO	Opaque dark blue	Mean	17.31	0.71	2.75	67.24	0.11	0.23	1.21	0.87	
		SD	0.11	0.02	0.06	0.47	0.01	0.06	0.07	0.04	0.01
S-BiBR-507-bi	Opaque white	Mean	16.53	5.01	1.95	67.19	0.04	0.27	0.85	0.52	6.23
		SD	0.20	0.06	0.06	0.38	0.04	0.05	0.04	0.01	0.03
S-BiBR-507-VT	Transparent green	Mean	14.54	3.11	1.97	56.69	1.14	0.15	1.01	1.77	8.64
		SD	0.13	0.11	0.07	0.25	0.06	0.03	0.07	0.01	0.09
S-BiR-507-bi	Opaque white	Mean	8.67	0.71	2.22	67.12	0.06	0.44	1.66	0.75	6.14
		SD	4.06	0.03	0.06	1.03	0.02	0.02	0.08	0.07	0.10
S-BT-004-BO	Opaque dark blue	Mean	15.92	0.55	2.39	68.02	0.03	0.28	1.20	0.56	4.13
		SD	0.54	0.01	0.12	1.16	0.03	0.07	0.22	0.01	0.14
S-BT-004-BT	Transparent dark blue	Mean	14.18	0.53	2.29	69.82	0.07	0.36	1.60	0.65	6.03
		SD	0.15	0.04	0.03	0.38	0.01	0.05	0.04	0.02	0.05
S-BT-004-T	True colorless	Mean	8.79	0.36	1.99	71.92	0.05	0.28	1.80	1.19	4.87
		SD	0.37	0.01	0.08	0.54	0.02	0.03	0.02	0.05	0.09
S-BTW-004-bi	Opaque white	Mean	11.67	0.74	2.00	60.07	0.19	0.29	0.68	0.64	4.03
		SD	0.29	0.03	0.03	0.69	0.05	0.06	0.02	0.02	0.08
S-BTW-004-BT	Transparent dark blue	Mean	14.23	0.64	1.89	71.01	0.06	0.28	1.55	0.84	3.26
		SD	0.31	0.03	0.04	0.71	0.03	0.08	0.17	0.03	0.05
S-BTW-004-W	Transparent dark blue	Mean	0.23	0.62	1.82	76.10	0.05	0.32	1.88	0.64	3.30
		SD	0.02	0.02	0.04	0.38	0.02	0.01	0.09	0.01	0.03
S-GA-005-A	Opaque light blue	Mean	16.05	0.42	1.83	70.51	0.04	0.18	1.25	0.36	4.50
		SD	0.24	0.04	0.01	0.48	0.02	0.04	0.05	0.01	0.06
S-GA-411-A	Opaque dark blue	Mean	14.78	0.60	2.52	69.45	0.20	0.23	0.85	0.64	8.02
		SD	0.29	0.01	0.02	0.24	0.02	0.03	0.01	0.01	0.07

TABLE 1 (Continued)

Sample name	Color		Na_2O	MgO	Al_2O_3	SiO_2	SO_3	P_2O_5	Cl	K_2O	CaO
S-GB-413-BO	Opaque dark blue	Mean	15.23	0.78	2.89	68.32	0.03	0.17	1.45	0.65	
		SD	0.45	0.03	0.02	0.36	0.04	0.01	0.03	0.05	0.03
S-GB-413-BT	Transparent dark blue	Mean	0.49	0.24	0.73	73.25	0.05	0.41	2.30	0.29	6.34
		SD	0.04	0.03	0.07	0.38	0.02	0.04	0.08	0.03	0.07
S-GRT-501-T	True colorless	Mean	9.14	1.78	1.93	43.81	0.74	0.34	0.79	1.26	5.73
		SD	0.18	0.03	0.03	0.23	0.03	0.07	0.02	0.02	0.08
S-RV-418-V	Opaque turquoise	Mean	16.54	0.55	1.74	69.36	0.12	0.42	0.79	0.63	5.94
		SD	0.40	0.01	0.11	0.38	0.02	0.02	0.02	0.01	0.06
S-TA-005-A	Opaque light blue	Mean	17.75	0.75	2.44	67.18	0.09	0.27	1.42	0.51	6.96
		SD	0.16	0.03	0.04	0.41	0.03	0.04	0.09	0.02	0.03
S-TA-005-T	True colorless	Mean	13.48	0.36	2.03	72.51	0.06	0.29	1.96	0.86	4.98
		SD	0.22	0.03	0.03	0.22	0.03	0.02	0.06	0.01	0.02
S-TR-501-T	True colorless	Mean	12.93	0.35	2.00	72.04	0.05	0.30	1.89	0.75	4.95
		SD	0.61	0.02	0.11	0.30	0.01	0.03	0.09	0.05	0.05
S-VA-405-B	Opaque dark blue	Mean	14.45	0.53	1.97	65.02	0.52	0.12	0.74	0.99	5.34
		SD	0.56	0.03	0.05	0.50	0.03	0.00	0.05	0.01	0.11
S-VA-405-A	Opaque turquoise	Mean	15.22	0.61	1.94	66.78	0.45	0.11	0.71	0.72	6.74
		SD	0.62	0.06	0.39	0.94	0.05	0.03	0.08	0.09	1.03

TABLE 1 (Continued)

Sample name	TiO_2	MnO	FeO	CoO	NiO	CuO	ZnO	As_2O_5	SnO_2	Sb_2O_5	PbO	Total
I-B-616	0.28	0.01	1.15	0.56	0.05	0.48	0.05	0.01	0.03	1.83	0.08	100.34
	0.03	0.01	0.11	0.06	0.03	0.08	0.05	0.01	0.03	0.05	0.13	
I-BBi-613-bi	0.12	1.46	0.81	0.00		0.06		0.01	0.13	6.65	7.28	101.40
	0.03	0.08	0.06	0.00		0.05		0.01	0.02	0.50	0.06	
I-BBi-613-BT	0.13	0.71	1.48	0.21	0.00	0.17	0.00	0.01	0.03	0.04	0.10	101.73
	0.05	0.04	0.16	0.04	0.00	0.01	0.01	0.03	0.03	0.03	0.02	
M-A-005	0.13	0.07	0.74	0.02	0.02	2.32	0.07	0.03	0.13	1.15	0.04	100.24
	0.03	0.02	0.04	0.02	0.03	0.03	0.05	0.02	0.05	0.09	0.07	
M-A-005a	0.18	0.24	1.28	0.04	0.06	2.65	0.02	0.22	0.20	1.26	1.17	100.75
	0.01	0.02	0.04	0.02	0.06	0.08	0.04	0.09	0.03	0.07	0.16	
M-A-006	0.07	0.74	0.56	0.01	0.03	1.66	0.04	0.00	0.04	2.62	8.35	99.86
	0.03	0.04	0.29	0.02	0.03	0.04	0.03	0.01	0.03	0.16	0.12	
M-B-002	0.05	0.29	1.77	0.29	0.00	0.44	0.02	0.01	0.02	2.12	10.48	97.96
	0.02	0.04	0.04	0.05	0.01	0.04	0.00	0.02	0.03	0.12	0.27	
M-B-004	0.06	0.01	1.04	0.04	0.01	0.23	0.02	0.01	0.02	0.60	0.06	98.01
	0.01	0.01	0.01	0.02	0.04	0.04	0.04	0.02	0.02	0.05	0.02	
M-BAu-002	0.05	0.47	1.35	0.88	0.03	1.01	0.03	0.06	0.09	4.16	0.00	102.70
	0.04	0.03	0.07	0.01	0.01	0.01	0.03	0.03	0.05	0.07	0.04	
M-T-503	0.19	1.32	1.28	0.01		0.06		0.02	0.02	0.20	0.18	100.94
	0.04	0.30	0.03	0.01		0.07		0.03	0.01	0.05	0.09	
M-T-503a	0.14	0.83	1.04	0.03		0.18		0.01	0.01	0.11	0.01	99.23
	0.00	0.03	0.04	0.05		0.05		0.01	0.02	0.05	0.02	
M-V-005	0.05	0.39	0.48	0.01		2.57		0.04	0.20	5.22	11.20	101.69
	0.04	0.03	0.01	0.01		0.05		0.04	0.05	1.48	0.31	
M-V-005a	0.13	0.87	0.65	0.04		5.48		0.01	0.61	2.13	5.49	100.32
	0.02	0.05	0.04	0.04		0.19		0.02	0.03	0.51	0.34	

TABLE 1 (Continued)

Sample name	TiO_2	MnO	FeO	CoO	NiO	CuO	ZnO	As_2O_5	SnO_2	Sb_2O_5	PbO	Total
M-V-006	0.10	0.75	0.32	0.02		2.95		0.03	0.01	2.87	0.18	99.63
	0.02	0.06	0.04	0.02		0.12		0.02	0.02	0.47	0.10	
M-V-006a	0.07	0.75	0.47	0.02	0.01	1.73	0.01	0.00	0.03	2.65	7.03	98.81
	0.05	0.04	0.04	0.02	0.01	0.02	0.02	0.01	0.02	0.29	0.43	
P-A-402-B	0.05	0.48	1.40	0.79	0.03	1.02	0.04	0.03	0.05	4.01	0.10	100.79
	0.02	0.01	0.06	0.04	0.04	0.15	0.05	0.03	0.03	0.06	0.06	
P-A-408-B	0.14	0.65	1.33	0.31	0.05	0.42	0.00	0.01	0.02	1.73	1.52	99.99
	0.04	0.01	0.02	0.03	0.03	0.05	0.00	0.01	0.02	0.12	0.22	
P-A-418-bi	0.12	0.03	0.61	0.01		0.00		0.02	0.02	4.32	0.11	102.32
	0.03	0.03	0.02	0.01		0.01		0.03	0.02	0.30	0.05	
P-A-418-BO	0.13	0.45	1.09	0.19	0.02	0.24	0.07	0.01	0.06	3.19	2.64	101.72
	0.02	0.02	0.08	0.02	0.02	0.05	0.07	0.01	0.02	0.08	0.37	
P-A-419-bi	0.10	0.09	0.73	0.04		0.05		0.05	0.21	5.36	7.07	101.29
	0.03	0.02	0.07	0.02		0.06		0.02	0.05	0.11	0.19	
P-A-419-BT	0.15	0.44	1.53	0.11	0.01	0.43	0.35	0.02	0.02	2.77	1.03	101.05
	0.05	0.03	0.06	0.04	0.02	0.06	0.27	0.02	0.02	0.07	0.10	
P-CR-421-A	0.13	0.03	0.52	0.03	0.03	2.95	0.08	0.01	0.14	1.80	0.07	101.08
	0.02	0.01	0.03	0.02	0.02	0.19	0.09	0.02	0.02	0.05	0.05	
P-CR-421-B	0.13	0.37	1.24	0.19	0.01	0.35	0.06	0.04	0.02	3.15	0.99	102.63
	0.02	0.06	0.03	0.04	0.02	0.05	0.05	0.05	0.01	0.06	0.19	
P-CR-421-bi	0.09	0.01	0.39	0.01		0.06		0.03	0.04	3.33	1.05	90.63
	0.02	0.01	0.01	0.01		0.04		0.02	0.02	0.06	0.07	
P-CR-421-BT	0.10	0.03	1.03	0.07		0.46		0.01	0.02	0.56	0.03	99.23
	0.03	0.03	0.06	0.04		0.09		0.02	0.02	0.02	0.04	

TABLE 1 (Continued)

Sample name	TiO_2	MnO	FeO	CoO	NiO	CuO	ZnO	As_2O_5	SnO_2	Sb_2O_5	PbO	Total
P-FL-004-B	0.20	0.09	2.36	0.20	0.01	0.41	0.04	0.01	0.01	2.71	0.19	102.27
	0.03	0.03	0.01	0.05	0.01	0.04	0.09	0.02	0.02	0.05	0.04	
P-FL-004-bi	0.07	0.04	0.34	0.01		0.04		0.03	0.01	2.97	0.01	102.88
	0.02	0.03	0.02	0.01		0.03		0.04	0.02	0.15	0.01	
P-FL-501-bi	0.14	0.07	0.63	0.00		0.03		0.04	0.03	5.93	0.31	98.94
	0.03	0.01	0.04	0.00		0.04		0.04	0.04	0.34	0.03	
P-FL-501-BT	0.20	0.95	1.46	0.05	0.02	0.18	0.04	0.02	0.00	0.16	0.05	100.17
	0.03	0.04	0.05	0.01	0.01	0.06	0.05	0.02	0.00	0.02	0.05	
P-FR-422-B	0.12	0.11	1.28	0.25	0.00	0.27	0.04	0.01	0.06	1.90	2.41	100.33
	0.01	0.02	0.06	0.05	0.00	0.02	0.03	0.01	0.04	0.16	0.05	
P-FR-422-bi	0.06	0.01	0.34	0.01		0.03		0.06	0.02	2.88	0.03	102.53
	0.02	0.02	0.04	0.01		0.02		0.05	0.02	0.19	0.03	
P-FR-422-T1	0.09	0.03	1.01	0.04		0.22		0.01	0.01	0.58	0.04	100.01
	0.02	0.03	0.04	0.03		0.05		0.01	0.01	0.02	0.05	
Pn-B-001	0.07	0.50	0.59	0.11	0.01	0.14	0.04	0.02	0.01	0.64	0.16	87.90
	0.04	0.04	0.01	0.04	0.01	0.05	0.04	0.03	0.02	0.07	0.04	
Pn-T-001	0.16	0.16	0.84	0.01		0.00		0.00	0.00	0.51	0.00	98.40
	0.06	0.05	0.06	0.01		0.00		0.00	0.00	0.09	0.00	
P-R-414-BO	0.21	0.14	2.52	0.26	0.02	0.40	0.04	0.02	0.03	2.65	0.27	103.29
	0.03	0.03	0.06	0.05	0.01	0.06	0.12	0.02	0.03	0.09	0.05	
P-R-414-T	0.08	0.03	0.37	0.01	0.01	0.04	0.03	0.00	0.00	0.81	0.00	101.27
	0.01	0.01	0.03	0.01	0.03	0.03	0.03	0.01	0.00	0.04	0.05	
P-R-419-BO	0.18	0.13	2.47	0.21	0.01	0.45	0.01	0.04	0.01	2.72	0.16	98.09
	0.02	0.03	0.07	0.03	0.00	0.08	0.01	0.03	0.02	0.20	0.02	

TABLE 1 (Continued)

Sample name	TiO_2	MnO	FeO	CoO	NiO	CuO	ZnO	As_2O_5	SnO_2	Sb_2O_5	PbO	Total
P-R-419-BT	0.08	0.02	1.03	0.05	0.00	0.63	0.00	0.00	0.01	0.54	0.11	99.41
	0.03	0.01	0.11	0.02	0.01	0.50	0.01	0.00	0.01	0.04	0.03	
P-R-419-VT	0.25	0.19	1.79	0.02		4.85		0.02	0.86	0.51	19.35	99.22
	0.05	0.04	0.05	0.03		0.10		0.03	0.06	0.03	0.52	
P-R-423-BO	0.19	0.14	2.41	0.21	0.02	0.45	0.03	0.04	0.03	2.58	0.23	101.84
	0.06	0.03	0.01	0.06	0.02	0.05	0.03	0.03	0.03	0.03	0.07	
P-R-423-BT	0.15	0.07	1.27	0.07	0.04	0.19	0.07	0.00	0.02	0.46	1.74	101.27
	0.04	0.01	0.06	0.02	0.04	0.03	0.07	0.00	0.02	0.05	0.40	
P-R-423-VT	0.22	0.33	1.40	0.02		0.13		0.04	0.00	0.09	0.08	102.50
	0.04	0.04	0.05	0.02		0.03		0.03	0.00	0.01	0.05	
P-St-415-B	0.17	0.05	1.90	0.30		0.42		0.05	0.05	3.75	0.94	99.93
	0.02	0.02	0.08	0.03		0.07		0.04	0.01	0.24	0.05	
P-St-415-bi	0.14	0.08	0.72	0.01	0.03	0.02	0.00	0.02	0.03	6.26	0.26	97.86
	0.03	0.03	0.07	0.02	0.04	0.03	0.02	0.02	0.01	0.67	0.02	
P-StB-002	0.08	0.94	2.22	0.36	0.02	0.50	0.04	0.03	0.04	3.62	0.83	101.06
	0.02	0.02	0.08	0.05	0.02	0.08	0.03	0.03	0.03	0.03	0.04	
P–T-417-bi	0.11	0.11	0.56	0.00		0.01		0.02	0.04	4.80	0.81	101.77
	0.01	0.01	0.05	0.00		0.02		0.03	0.03	1.45	0.21	
P–T-417-BO	0.09	0.41	0.93	0.08	0.00	0.90	0.04	0.00	0.06	5.43	4.72	103.07
	0.01	0.06	0.06	0.04	0.00	0.07	0.05	0.00	0.03	0.84	0.30	
P–T-417-VT	0.05	0.95	1.37	0.01		0.02		0.00	0.00	0.11	0.02	100.45
	0.03	0.05	0.02	0.00		0.03		0.01	0.00	0.03	0.04	
S-423a-A	0.04	0.04	0.30	0.01	0.01	3.80	0.00	0.02	0.24	1.57	0.01	97.48
	0.04	0.02	0.02	0.02	0.02	0.08	0.00	0.01	0.04	0.08	0.04	

TABLE 1 (Continued)

Sample name	TiO_2	MnO	FeO	CoO	NiO	CuO	ZnO	As_2O_5	SnO_2	Sb_2O_5	PbO	Total
S-423a-bi	0.07	0.06	0.32	0.02		0.08		0.04	0.02	2.87	0.01	101.60
	0.02	0.01	0.02	0.02		0.00		0.04	0.02	0.07	0.05	
S-423a-T	0.09	0.02	0.84	0.05		0.44		0.02	0.00	0.57	0.12	97.53
	0.04	0.02	0.04	0.03		0.07		0.03	0.01	0.01	0.01	
S-ARG-403-A	0.07	0.03	0.52	0.00	0.03	3.36	0.09	0.02	0.14	1.84	0.20	100.56
	0.01	0.03	0.03	0.00	0.03	0.12	0.04	0.02	0.03	0.34	0.08	
Sb-B-003	0.08	0.58	0.32	0.15	0.02	0.04	0.02	0.01	0.04	0.03	0.13	99.03
	0.04	0.03	0.08	0.05	0.03	0.03	0.02	0.01	0.05	0.02	0.02	
S-BB-004-BO	0.19	0.13	2.33	0.20	0.01	0.41	0.04	0.05	0.03	2.55	0.32	100.49
	0.05	0.03	0.11	0.03	0.02	0.03	0.05	0.04	0.01	0.02	0.02	
S-BB-004-BT	0.08	0.04	0.99	0.15	0.01	0.23	0.03	0.01	0.01	0.82	0.10	97.55
	0.03	0.04	0.04	0.03	0.00	0.04	0.04	0.02	0.01	0.02	0.10	
S-BBi-004-bi	0.19	0.44	0.60	0.03		0.03		0.00	0.03	4.16	0.72	100.17
	0.05	0.02	0.07	0.05		0.03		0.00	0.03	3.78	0.03	
S-BBi-004-BT	0.16	0.91	1.66	0.26	0.00	0.37	0.06	0.00	0.00	0.02	0.03	99.74
	0.02	0.39	0.10	0.27	0.00	0.45	0.06	0.00	0.01	0.03	0.04	
S-BBi-004-BTc	0.16	1.33	1.44	0.55	0.04	0.90	0.05	0.01	0.01	0.13	0.04	100.24
	0.03	0.05	0.07	0.03	0.04	0.00	0.06	0.01	0.01	0.06	0.07	
S-BBi-004-BTs	0.12	0.73	1.85	0.10	0.02	0.15	0.02	0.03	0.02	0.00	0.00	100.65
	0.01	0.01	0.01	0.04	0.01	0.05	0.01	0.03	0.03	0.00	0.05	
S-BiBR-404-bi	0.09	0.02	0.39	0.01		0.01		0.05	0.01	3.00	0.01	102.34
	0.05	0.03	0.02	0.01		0.02		0.01	0.02	0.21	0.04	
S-BiBR-404-BO	0.21	0.13	2.47	0.25	0.01	0.46	0.02	0.01	0.01	2.67	0.20	102.05
	0.05	0.03	0.10	0.04	0.01	0.05	0.02	0.01	0.01	0.12	0.09	

TABLE 1 (Continued)

Sample name	TiO_2	MnO	FeO	CoO	NiO	CuO	ZnO	As_2O_5	SnO_2	Sb_2O_5	PbO	Total
S-BiBR-507-bi	0.05	0.01	0.39	0.01		0.04		0.03	0.01	2.86	0.04	102.04
	0.01	0.03	0.03	0.02		0.05		0.03	0.01	0.12	0.04	
S-BiBR-507-VT	0.18	0.43	1.61	0.01		0.30		0.00	0.32	0.21	8.55	100.62
	0.03	0.07	0.08	0.01		0.08		0.01	0.05	0.02	0.15	
S-BiR-507-bi	0.13	0.02	0.65	0.01		0.01		0.01	0.03	3.37	0.03	92.02
	0.03	0.03	0.01	0.02		0.02		0.01	0.02	0.69	0.05	
S-BT-004-BO	0.15	0.05	1.51	0.16	0.01	0.35	0.02	0.03	0.02	2.90	0.51	98.74
	0.03	0.01	0.08	0.01	0.01	0.13	0.02	0.02	0.03	0.10	0.15	
S-BT-004-BT	0.09	0.02	1.05	0.18	0.02	0.17	0.02	0.02	0.02	0.84	0.14	98.07
	0.03	0.02	0.03	0.04	0.01	0.02	0.02	0.03	0.02	0.03	0.07	
S-BT-004-T	0.06	0.01	0.24	0.01		0.01		0.02	0.01	0.75	0.06	92.43
	0.05	0.01	0.05	0.02		0.01		0.03	0.01	0.02	0.05	
S-BTW-004-bi	0.19	0.70	0.83	0.04		0.06		0.03	0.18	5.24	12.55	100.12
	0.07	0.05	0.03	0.04		0.05		0.03	0.05	0.23	0.46	
S-BTW-004-BT	0.24	1.01	1.50	0.33	0.03	0.42	0.00	0.01	0.02	0.24	0.00	97.52
	0.03	0.05	0.03	0.02	0.01	0.07	0.00	0.02	0.01	0.03	0.02	
S-BTW-004-W	0.28	1.10	1.59	0.35		0.34		0.01	0.01	0.19	0.02	88.84
	0.04	0.04	0.06	0.04		0.03		0.03	0.02	0.02	0.04	
S-GA-005-A	0.07	0.04	0.86	0.02	0.01	2.64	0.05	0.27	0.20	1.99	0.39	101.68
	0.04	0.01	0.02	0.02	0.02	0.10	0.03	0.04	0.02	0.06	0.08	
S-GA-411-A	0.07	0.33	0.79	0.06	0.03	0.06	0.05	0.01	0.01	2.26	0.07	101.02
	0.07	0.03	0.04	0.04	0.02	0.04	0.06	0.01	0.01	0.03	0.09	
S-GB-413-BO	0.25	0.17	1.92	0.32	0.03	0.44	0.05	0.06	0.03	3.06	0.25	99.47
	0.01	0.03	0.04	0.04	0.03	0.05	0.06	0.02	0.04	0.12	0.05	

TABLE 1 (Continued)

Sample name	TiO_2	MnO	FeO	CoO	NiO	CuO	ZnO	As_2O_5	SnO_2	Sb_2O_5	PbO	Total
S-GB-413-BT	0.06	0.07	0.98	0.30	0.01	0.32	0.04	0.01	0.01	0.00	0.04	85.95
	0.03	0.01	0.02	0.08	0.00	0.03	0.03	0.01	0.01	0.00	0.08	
S-GRT-501-T	0.20	0.43	1.48	0.04		5.35		0.04	1.27	0.42	24.19	98.92
	0.02	0.06	0.07	0.05		0.20		0.05	0.06	0.03	0.52	
S-RV-418-V	0.08	0.29	0.65	0.01		2.23		0.00	0.19	2.39	0.32	102.26
	0.04	0.04	0.08	0.01		0.07		0.00	0.03	0.23	0.03	
S-TA-005-A	0.13	0.05	0.71	0.02	0.01	2.24	0.21	0.03	0.09	1.21	0.05	102.11
	0.04	0.01	0.05	0.02	0.02	0.03	0.20	0.02	0.02	0.09	0.04	
S-TA-005-T	0.08	0.02	0.28	0.01		0.02		0.01	0.01	0.72	0.01	97.68
	0.02	0.03	0.03	0.02		0.03		0.01	0.01	0.02	0.09	
S-TR-501-T	0.02	0.00	0.29	0.00		0.00		0.01	0.02	0.75	0.00	96.35
	0.03	0.00	0.04	0.00		0.00		0.01	0.03	0.03	0.00	
S-VA-405-B	0.24	0.28	1.46	0.15	0.00	0.49	0.03	0.01	0.04	6.07	0.15	98.56
	0.03	0.02	0.04	0.03	0.00	0.05	0.05	0.00	0.02	0.38	0.13	
S-VA-405-A	0.11	0.19	0.51	0.00	0.00	1.59	0.02	0.02	0.10	2.30	0.69	98.80
	0.04	0.02	0.03	0.00	0.01	0.13	0.00	0.00	0.11	0.17	0.31	

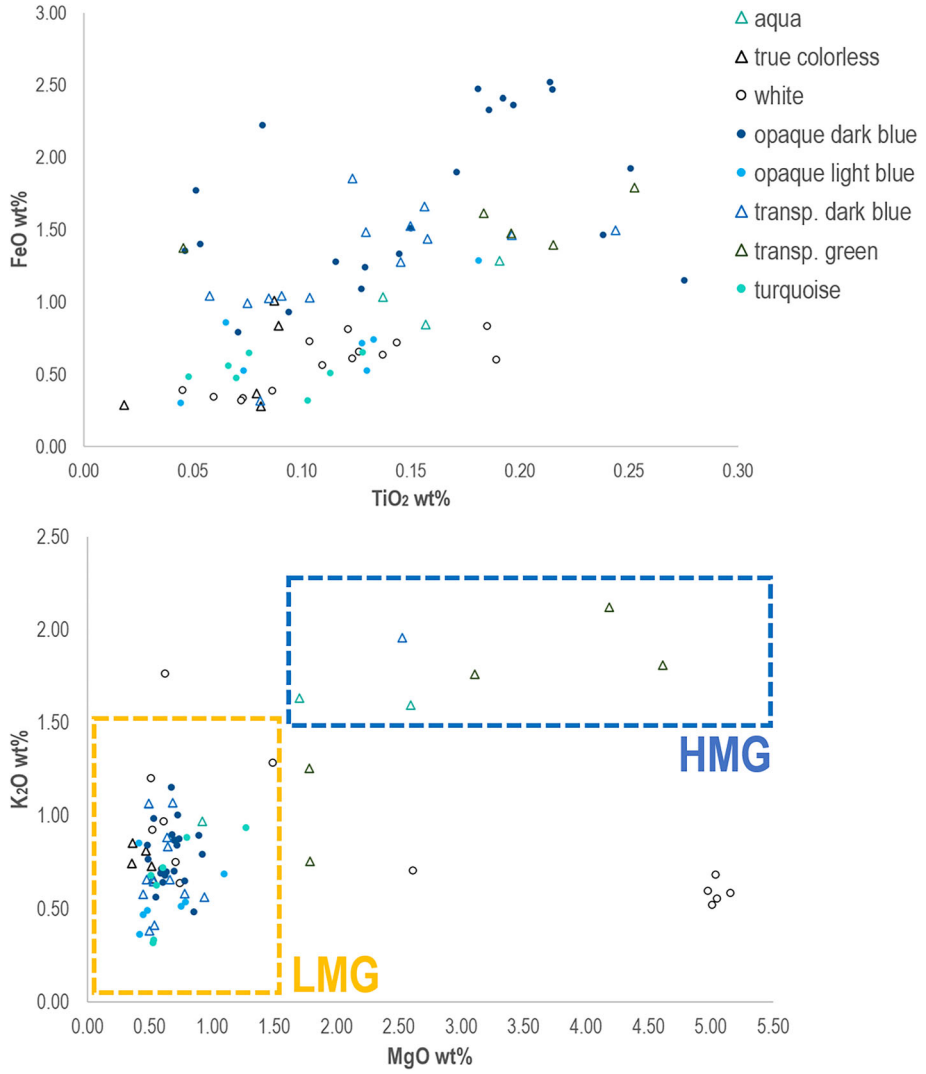

FIGURE 2 (a) TiO_2 versus FeO contents in the glass phase of the analyzed samples from Tebtynis. (b) K_2O versus MgO content of the glass phase in the analyzed samples from Tebtynis (excluding weathered glasses). Compositional fields of HMG and LMG glasses (dotted lines) refer to (Henderson, 2013). Symbols: empty triangles, transparent glasses; colored dots and asterisks, opaque glasses; the color of the symbols is related to the color seen during macroscopic observations

A few transparent blue, green, and colorless glasses from Tebtynis were instead produced with the typical recipe of high-magnesium glasses (HMG), obtained using soda-rich plant ash as flux (Henderson, 1988, 2000; Shortland & Eremin, 2006). This second class presents higher levels of both K_2O (1.60–2.12%), MgO (1.70–4.61%), and comparable Na_2O (14.36–17.19%).

Despite the lack of a systematic association between color and lead content, the ratio Na_2O/PbO (Table 1) shows that blue and white samples tend to have low, or even absent, PbO, while various transparent green and turquoise samples are characterized by a content of PbO > 1.5% (specifically between 1.52% and up to 24.19%).

Coloring, decoloring, and opacifying agents

Colorless glasses

Two color categories are included in this class: true colorless glasses (six samples) and naturally colored glasses (three samples), which were labeled as "aqua". Colorless samples from Tebtynis show very low values of intentionally added chromophores, such as CuO (from under detection limit to 0.22%), CoO (from under detection limit to 0.04%), while FeO is very variable, ranging from 0.24% to 1.28%, but is systematically higher in aqua samples (0.84–1.28 wt%).

In the HMG class, MnO ranges from 0.83% to 1.31%, with low Sb_2O_5 between 0.11% and 0.20%. Conversely, LMG glasses have higher Sb_2O_5 (0.51–0.81%) and much lower MnO, from under the detection limit to 0.03%, except in the aqua sample, where it reaches values of 0.16%. From the textural point of view, all the samples are essentially homogeneous with rare bubbles up to 100 μm in size.

White glasses

In the Tebtynis collection, opaque white glass was only found in stratified and mosaic compositions and never on its own. Of the 14 analyzed samples, one comes from a figured inlay, five from stratified samples, and all others (eight samples) from complex mosaic glasses.

Considering the K_2O versus MgO content, two main clusters appear quite clearly: the first is a uniform high MgO (from 4.98% to 5.16%), low K_2O (0.52–0.60%) group, already mentioned in the alkali source section (Section 3.2). All other samples are classic LMG glasses, with a subset characterized by high lead (7.07–12.55 wt%) and proportionally higher levels of tin (0.13–0.21 wt%) and manganese (0.44–1.46 wt%) content compared to the non-leaded LMG glasses.

All samples have significant levels of both CaO and Sb_2O_5, in the range of 3.48–7.98% and 2.86–6.65%, respectively. These values are consistent with the textural and chemical analyses, which revealed a diffuse presence of Ca antimonates dispersed in the glassy matrix as opacifying agents. Synthetic crystals of euhedral brizziite ($NaSbO_3$) were also found in sample S-BiR-507, as confirmed by the μ-Raman spectra (Figure 3a). Wavelength-dispersive X-ray spectroscopy (WDS) data on the biggest crystal returned an Na_2O value of 18.5% with Sb_2O_5 at 82.66%, which is compatible with the microprobe analysis performed on the natural brizziite samples at the time of its discovery (Olmi & Sabelli, 1994). Unfortunately, the glassy matrix of this sample is slightly weathered, and it is not possible to establish a connection with the exact original alkali composition to understand what favored the precipitation of this specific phase, in contrast to the classic calcium antimonate compounds, since CaO in the glassy matrix is sufficiently high (6.14%).

Calcium antimonates exist in two spatial configurations: $Ca_2Sb_2O_7$ (orthorhombic structure) and $CaSb_2O_6$ (hexagonal structure). Raman data showed that $CaSb_2O_6$ and $Ca_2Sb_2O_7$ are not the only Ca antimonates present in the white glasses from Tebtynis: sample P-CR-421-Bi has both euhedral and "rosary"-shaped crystals similar to the classic morphologies and sizes of $CaSb_2O_6$ and $Ca_2Sb_2O_7$ phases, which returned the spectrum of the mineral romeite, i.e. $(Ca, Mn, Fe, Na)_2(Sb, Ti)_2O_6(OH, F, O)$.

Blue glasses

All analyzed blue samples, regardless of their shade and/or opacity, are colored with cobalt, copper, or a combination of the two chromophores. The main chemical zonings of

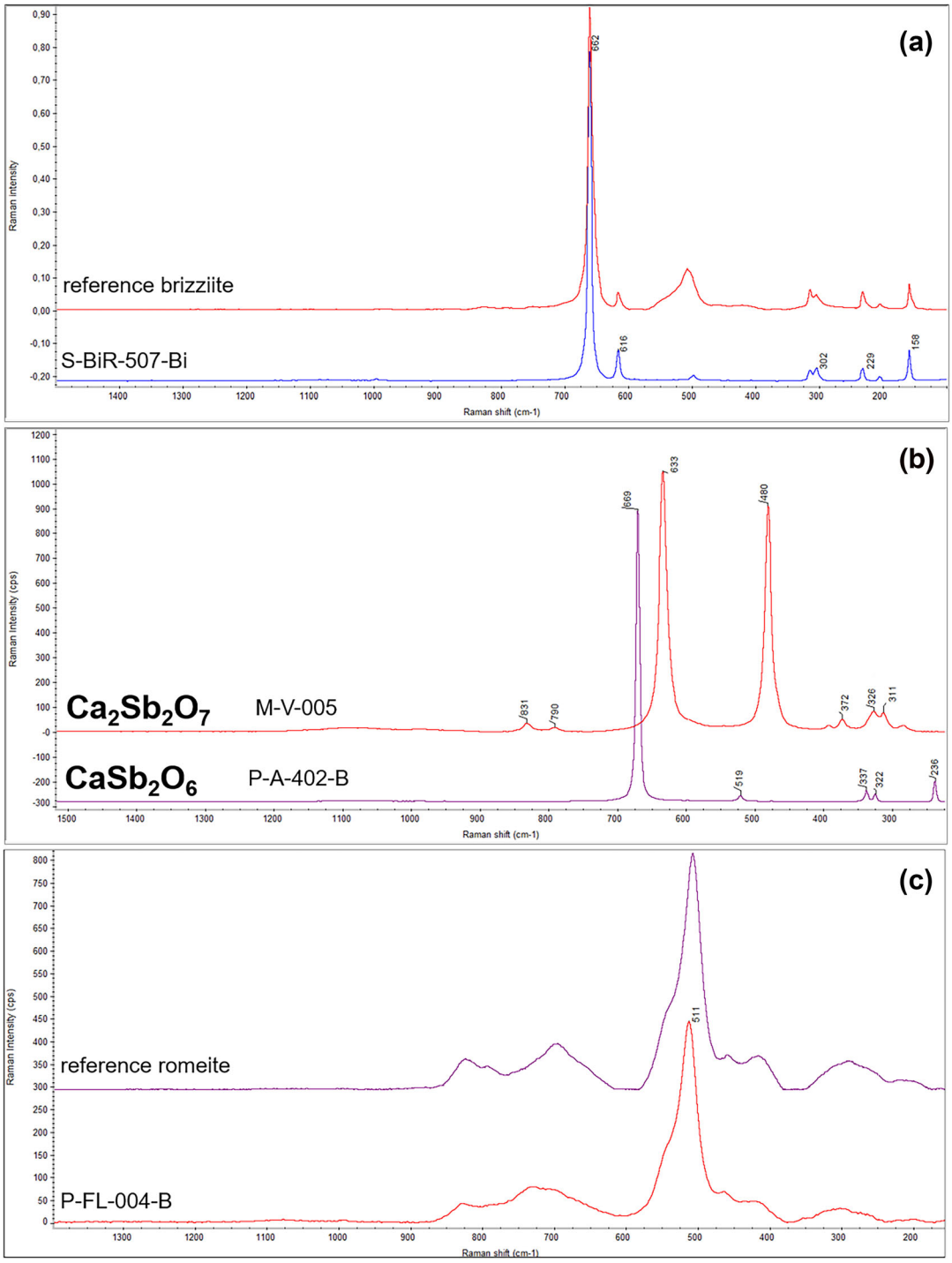

FIGURE 3 Raman spectra with standard reference spectra (RRUFF web database) of: (a) brizziite crystal in the white sample S-BiR-507-bi; (b) pure phases of $Ca_2Sb_2O_7$ (orthorhombic) in the turquoise sample M-V-005 and $CaSb_2O_6$ (hexagonal) in the dark blue sample P-A-402-B; (c) romeite crystal in the dark blue sample P-FL-004-B

heterogeneous glasses were also characterized by WDS. Observing the considered samples, three compositional groups can be identified (Figure 4). Group 1 comprises seven LMG glasses characterized by very low levels of CoO (from under detection limit to 0.04%), Sb_2O_5 between 1.15% and 1.99%, and high amounts of copper (2.24–3.80 wt%). Group 1 perfectly corresponds to the opaque light blue class, as defined by macroscopic observations. The second group is represented by 10 LMG and one HMG (Cu)Co-colored glasses, all with CoO between 0.04% and 0.55%, low CuO (from under detection limit to 0.90%), and Sb_2O_5 never exceeding 0.88%. Group 2 matches well with the "transparent dark blue" color class, except for sample P-A-419-BT, which has significantly higher antimony levels (2.77 wt%). Group 3 is constituted by 22 LMG glasses that show Sb_2O_5 of the order of 1.73–6.07%, traces or low amounts of CuO (0.06–1.21%), and CoO (0.06–0.88%) mainly around 0.2–0.4%. This group fits with the opaque dark blue class observed before sampling and can be interpreted as similar to the (Cu)Co-colored group 2, with the addition of antimony-based opacifiers.

As for the texture, group 2 (plus sample P-A-419-BT, as noted above) is characterized by no intentional opacifying agent. The only exception is P-A-419-BT itself, which presents very few, localized, micrometric, and sub-micrometric calcium antimonate inclusions (EDS data) possibly precipitated from the Ca-Sb-rich glassy matrix.

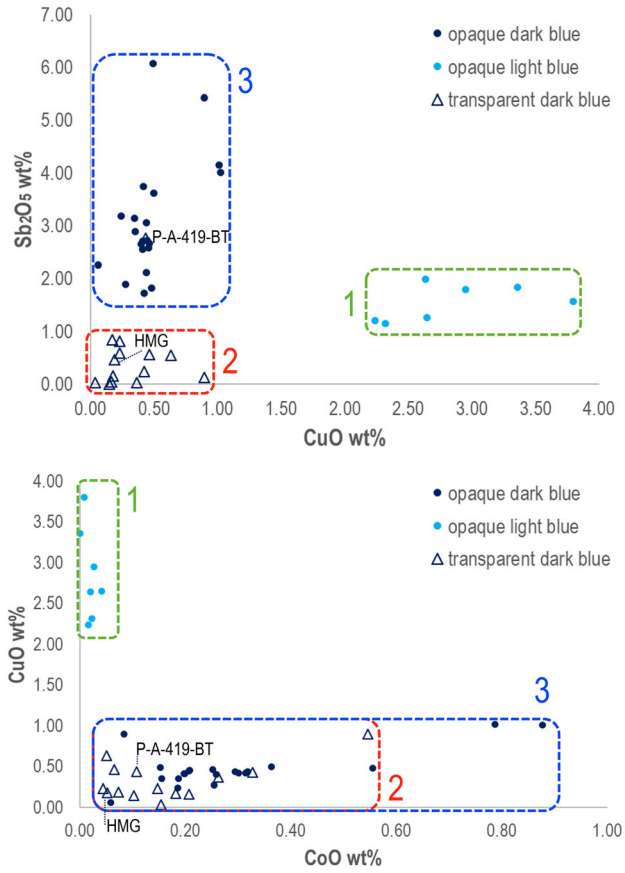

FIGURE 4 Sb_2O_5 versus CuO (top) and CuO versus CoO (bottom) binary plots of the glass phase in the Tebtynis blue samples. Dotted lines represent the three compositional groups identified. Symbols: empty triangles, transparent glasses; colored dots, opaque glasses; the colors of the symbols are related to the colors observed during macroscopic observations

The texture of transparent blue glasses is generally very uniform, but sample S-BBi-004-BT shows a peculiar zoning in BSE which can be interpreted as the result of an imperfect mixing. From dark to pale gray in Figure 5a, the coloring agents vary respectively in the ranges CuO 0.15–0.37%, CoO 0.10–0.26%, MnO 0.73–0.91%, and FeO 1.85–1.66% (WDS data).

The microstructure of opaque light blue and dark blue glasses is characterized by the presence of both Na and Ca antimonates (sometimes in solid solution), with one single analyzed case of Pb-doped Ca antimonate. Hexagonal $CaSb_2O_6$ and orthorhombic $Ca_2Sb_2O_7$ are both present in Tebtynis samples, irrespectively of the macroscopic color or the CuO/CoO rate in the glassy matrix (Figure 3b).

One dark blue sample (S-GB-413-BO) was again found to be opacified using synthetic brizziite ($Na_2O = 17.05\%$; $Sb_2O_5 = 83.76\%$). Romeite was found in light blue samples associated with brizziite (M-A-005) and $CaSb_2O_6$ (M-A-005 and M-A-005a), but also in one aggregate in the dark blue sample P-CR-421-B (Figure 3c).

Green glasses

Green glasses can be divided into two main categories according to their color intensity and opacity: transparent green (five samples) and opaque turquoise (seven samples). Just as in the case of white glasses, transparent greens were never found alone but always associated with

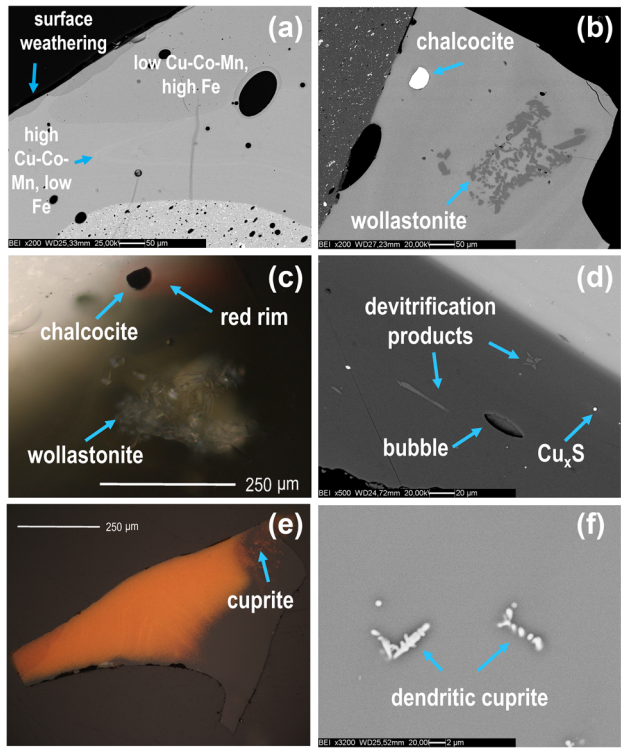

FIGURE 5 (a) Chemical zoning in sample S-BBi-004-BT (BSE image). (b,c) OM-RL-XPL and SEM-BSE image of a wollastonite aggregate associated with a 50 µm chalcocite drop (WDS data) in sample S-BiBR-507-VT. (d) Sample P-R-423-VT, chalcocite, devitrification products, and cu-Fe and Pb sulfides dispersed in the glassy matrix. (e,f) Nucleation of dendritic cuprite crystals at the interface with a yellowish-orange glass in P-R-419-VT (OM-RL with shifted nicols and SEM-BSE images)

other colors to create stratified or mosaic patterns. Conversely, turquoise samples are found both alone in bars, inlays, and polychrome compositions.

The chemical composition of this group is very heterogeneous, comprising at least three main classes:

1. Three transparent green glasses show no other ionic chromophore in significant concentrations, except for FeO (1.37–1.61%), which can thus be considered as their main coloring agent. Moreover, these glasses have high MgO (3.11–4.19%), CaO (8.51–9.99%), SO_3 (1.14–1.74%), and K_2O (1.77–2.12%) with respect to all other samples and can be thus interpreted as HMG glasses.
2. The two remaining transparent glasses (S-GRT-501-T and P-R-419-VT) are characterized by high amounts of CuO (4.85–4.35%) and PbO (19.35–24.19%). Considering their low K_2O (0.76% and 1.26%, respectively) and the average concentration of MgO (1.78%) they can be interpreted as leaded-LMG glasses.
3. The last set corresponds well to the color class of turquoise glasses, with very low FeO (0.32–0.65%), and medium to high copper (CuO 1.59–5.48%, with an average of 2.60%). The greenish hue must thus be attributed to copper, with a limited iron contribution. This group can be distinguished from the others also for the significant levels of antimony between 2.13% and 5.22 wt%. Lead is present in high concentrations in the glassy matrix of four turquoise samples (PbO 5.49–11.20%), while the remaining three turquoise glasses have only traces or minor contents (0.18–0.69%).

As already noted, copper in turquoise samples is always associated with antimony and varying quantities of CaO (2.01–7.91 wt%), which are related to opacifiers dispersed in the glassy matrix. Examination via SEM-EDS confirmed the presence of calcium antimonate inclusions, often in solid solution with sodium (in M-V-006a and M-A-006) and small amounts of lead, reaching up to 3.6 wt%. The μ-Raman analyses confirmed the presence of pure Ca antimonates in hexagonal ($CaSb_2O_6$) and orthorhombic ($Ca_2Sb_2O_7$) forms.

Coming to the transparent green glasses, as expected, the texture is generally homogeneous with limited or no porosity and no intentional opacifiers. However, three samples show peculiar inclusions (Figure 5b–f): S-BiBR-507-VT has a cluster of wollastonite crystals measuring ~250 × 100 μm and a 50 μm drop in chalcocite (Cu_2S, WDS data); OM-RL-XPL images show a red rim surrounding the copper sulfide inclusion. P-R-423-VT has small copper sulfide drops of 1–2 μm in diameter (probably chalcocite; EDS data), associated with one Cu-Fe and Pb sulfide (possibly chalcopyrite and galena; EDS data), and various Ca-P-Na silicates that can be interpreted as devitrification products. Finally, P-R-419-VT is characterized by the nucleation of small dendritic crystals of cuprous oxide (synthetic cuprite) growing at the interface with a yellowish-orange glass and thus suggesting that this kind of composition could have been used as the base glass for red and yellowish-orange glasses.

DISCUSSION

Base glass

Looking at Tebtynis samples, both chemical analyses and mineralogical characterization of the crystalline inclusions agree in suggesting that sand was the main silica source used to produce the base glass. The sources of sand employed by the ancient Egyptian glassmakers are not readily known. Turner (1956) and Lucas (Lucas & Harris, 1962) reviewed the analyses available at that time and concluded that Egyptian sands show wide geographical differences, considering the contents of the main constituents (SiO_2, Al_2O_3, Fe_2O_3, CaO, and minor MgO, K_2O). In

particular, they pointed out that seashore sands near Alexandria and around the Red Sea are very calcareous (CaO up to 34%) and of high purity ($Al_2O_3 + Fe_2O_3 = 0.70\%$), and those from the Fayoum oasis or Hermopolis Magna, in Upper Egypt, are essentially pure silica sand, with SiO_2 around 95% and moderate Al_2O_3/Fe_2O_3 contributions.

The high concentration and the linear correlation of iron and titanium, and the abundant ilmenite, iron oxides, corundum, and zircon in Tebtynis glass samples, imply the use of sands rich in heavy minerals, which are often associated with detrital sediments typical of coastal sands (Aerts et al., 2003; Deer et al., 2013). Mohamed E. Hilmy (1951) stated that the western Mediterranean coast of Egypt presents two different types of sands: calcareous (from the Libyan border to the beginning of the delta) and quartz-dominant, with frequent marine shells and abundant heavy minerals derived from Nile sediments transported from the Abyssinian plateau (from Alexandria to Rosetta). However, he notes that local differences are rather frequent. A few years later, El-Hinnawi (1964) published a mineralogical and geochemical survey on the gray and black sands of the Nile Delta, evidencing a significant concentration of heavy minerals, particularly ilmenite and magnetite, which were the major phases identified. Moreover, he found zircon, representing ~7% of the total heavy mineral fraction, garnet (2%), monazite (1%), and rutile (1%).

These last data are well consistent with the analyses of the Tebtynis glass samples, even if they cannot be used to demonstrate unequivocally a direct connection with the Mediterranean sands of the Nile Delta. Heavy minerals are rather common throughout Egypt: ilmenite, magnetite, rutile, and zircon (among others) were found in desert dunes in Lower Egypt, between Dayrut and Minya, together with carbonates and feldspars such as orthoclase, microcline, and sodic plagioclase (Takla & Arafa, 1975). Nevertheless, the light fraction of the considered sand is essentially composed of quartz (93%) and lacks significant quantities of Ca or Mg carbonates, which are fundamental as stabilizers for glassmaking. This problem could, however, be overcome by the deliberate addition of lime to the batch (Silvestri et al., 2006).

Given the peculiar association of heavy minerals in the Tebtynis samples, the base glass was probably produced with Egyptian sands (or with a mix of Egyptian and foreign sands) because the shoreline deposits of the Syro-Palestinian coast are generally characterized by higher purity (Degryse, 2014; Degryse et al., 2009; Turner, 1956). These considerations are also strengthened by the results of trace element analyses by laser ablation inductively coupled plasma mass spectrometry (LA-ICP-MS) published by Nenna and Gratuze (2009) for a different set of samples from Tebtynis, which highlighted ZrO between ~60 and 130 ppm. However, further LA-ICP-MS analyses are expected on our samples in the next steps of the project for a better contextualization of the provenance issues.

As previously noted, most of the colorless, blue, and green glasses from Tebtynis can be classified as natron glasses, with only a limited number of samples certainly associated with plant ash flux. The use of evaporitic salts as a fluxing agent for vitreous materials has a long tradition in Ancient Egypt, being first testified in the production of Predynastic glazed steatite (Tite et al., 2008). However, judging from the analyses of the Late Bronze Age (LBA) glasses, there is very limited evidence that natron might have been used at the dawn of the glass technology (e.g., Mass et al., 2002; Shortland & Eremin, 2006). The effective transition from plant ash to natron glass seems to have started in the Third Intermediate Period, around the 10th century BCE, and was essentially accomplished in its main terms by the 8th century BCE, both in Egypt and the Mediterranean (Sayre & Smith, 1961). However, it was during the mid-1st millennium BCE and throughout the Roman rule that natron became the standard flux for glass production, only to be replaced again by plant ashes around the 8th century CE (Angelini et al., 2019).

The anomalous group of five white glasses with very high MgO and low K_2O mentioned in Section 3.2 appears as a separate subset of LMG glasses, possibly in excess of stabilizers. However, it is not possible to discard the possibility of the use of plant ashes particularly low in potash (Barkoudah & Henderson, 2006, and references cited therein). Henderson (2013) proposed

the use of a mixture of natron and plant ash glass for a group of Early Medieval, white glasses from the Netherlands with unusually high MgO levels compared to the K_2O content. Considering the very low levels of FeO and TiO_2 in all the Mg-rich Tebtynis samples, which suggest the use of pure/purified sands, it would seem unlikely that they were all produced using mixtures of glasses with different alkali sources but with equally pure sands. A combined contribution of the two alkali sources cannot be excluded, even if the Tebtynis samples seem more probably associated with an addition of stabilizers, possibly connected to the coloring process. Addition of talc has already been suggested by Fiori (2015) for a Byzantine mosaic *tessera* with high Mg and very low K.

Coloring, decoloring, and opacifying agents

Colorless glasses

The principal component analysis (PCA) of colorless glasses (see Supporting Information, Figure S1) shows three well-defined compositional groups: the first comprises two of the three aqua glasses. Considering the association with MgO, K_2O, P_2O_3 and MnO in the loading plot, these two samples stand out as Mn-decolored HMG glasses in contrast with all other samples. The second and the third groups show the chemical signature of Sb-decolored LMG glasses with essentially no MnO (note that antimony and manganese are anticorrelated in the loading plot). However, they can be distinguished for peculiar differences especially in content of Na_2O (average in group 2 = 16.02% and in group 3 = 11.73%) and FeO (on average, 0.74% vs. 0.27%, respectively). The last aqua sample (Pn-T-001) is rather isolated in the score plot, due to the presence of both Sb and Mn.

Colorless glass is known from the LBA in Egypt and the Near East: from a compositional point of view, it was associated with very low levels of FeO and no deliberately added chromatophores. This is consistent with the use of very pure sands or, more probably, quartzite pebbles as silica source (Push & Rehren, 2007). The comprehensive review of Gliozzo (2017) on colorless glass and the data from other analytical studies (among others: Foster & Jackson, 2009; Paynter & Jackson, 2019; Schibille et al., 2017) indicated significant trends in the popularity of the decoloring agents: antimony is usually found in pre-Hellenistic productions and is widespread during the Roman and Late Antique periods. Conversely, manganese is typical of the Hellenistic and Early Roman phases, but is also frequent in Imperial glasses and returns as the main decolorant in Medieval times. The presence of both antimony and manganese in non-negligible concentrations, such as in Pn-T-001, a lump of twisted bars ready for reheating discovered in Tebtynis (Sb_2O_5 = 0.51%, MnO 0.16%), is generally considered as a marker of recycling, in perfect accordance with the functional attribution of the object (Figure 6).

The results obtained on the colorless (and slightly colored) samples from Tebtynis were compared with those analyzed from the site of Bubastis (Figure 6), in the Eastern Nile Delta (Rosenow & Rehren, 2014). It should, however, be noted that the glass from Bubastis is related to Late Hellenistic and Roman vessels, with a chronological range from the 1st century BCE to the 3rd century CE (typological dating), and thus the samples are generally more recent than those from Tebtynis. Moreover, vessel glass, especially if blown, may have particular chemical features for improving its workability (especially in rheological terms). However, given the lack of analytical data from Ptolemaic Egypt, the Bubastis glass offers the chance to evaluate the similarities and differences in the glass composition of two Graeco-Roman sites in Egypt.

Looking at the content of K_2O versus MgO and Sb_2O_3 versus MnO, the picture is rather clear: in both sites, natron-type and plant ash-type recipes coexist, with LMG glasses significantly prevailing. HMG samples tend to have high levels of manganese (of the order of

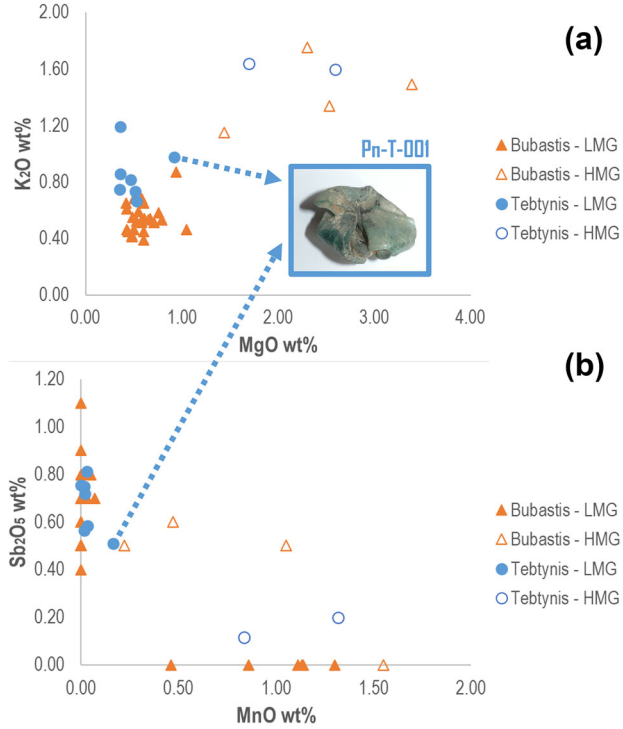

FIGURE 6 (a,b) K_2O versus MgO and Sb_2O_5 versus MnO contents of the glass phase in the Tebtynis glasses (blue dots) compared with those of Bubastis samples published in Rosenow and Rehren (2014) (orange triangles). Symbols: color-filled, LMG glasses; empty, HMG glasses

0.5–1.5 wt%) and variable antimony content. The good correlation of the samples from both sites, also in terms of major, minor, and partly trace elements, may testify to the existence of a long-lasting but small-scale tradition and/or the trade of HMG glass coexisting with the industrial-scale LMG production typical of the Graeco-Roman world.

Opaque white glasses

All the 14 white glasses analyzed in this work were sampled from polychrome objects in stratified and mosaic compositions. Again, the PCA of our samples proved to be an effective tool for the identification of compositional assemblages, as it highlighted very clearly three different classes (Supporting Information, Figure S2): (1) classic LMG glasses, with one single example (P–T-417-Bi) of an intermediate K-rich composition ($K_2O = 1.77\%$, $MgO = 0.62\%$); (2) soda-lime-lead and leaded LMG glasses; (3) low-K and Mg-rich glasses, having higher levels of soda and stabilizers.

The composition of Mg-rich glasses (group 3) is similar to HMG glasses, but the very low potash may indicate a different recipe. The low levels of FeO seen in this class can no doubt be associated with the use of a very pure silica source. Hence the very high levels and the correlation between the CaO and MgO concentrations (with an average Ca/Mg elemental ratio of 1.4) and the lack of any association between K_2O/MgO may be the effect of a voluntary addition, deriving from a Ca- and Mg-rich source, such as dolomitic limestone, which can be found in several outcrops in the Nile valley or the Eastern and Western deserts (Rapp, 2017).

Summing up, it is argued that Mg-rich glasses probably constitute a subset of natron glasses produced by adding high quantities of CaO and MgO from the same or from two correlated sources to pure/purified sands.

One white glass (P-A-418-Bi) has an intermediate composition between LMG and Mg-rich glasses. However, judging from its overall composition, this sample fits relatively well in the latter group, even if the magnesia levels are slightly lower (2.61%) and lime is proportionally higher (7.89%), totaling ~11% CaO + MgO (as typical of this group), thus suggesting that the stabilizers were added using raw materials with different Ca/Mg proportions.

Antimonate-based opacifiers in white and blue glasses

Antimony-based minerals are the main phases responsible for glass opacification in white, blue, green, and yellow glasses since the LBA and are systematically substituted by tin-based opacifiers only in the 4th century BCE, despite some earlier occurrences testified during the Iron Age (Tite, Pradell, & Shortland, 2008; Van Ham-Meert et al., 2019). It is no surprise that all opaque white, blue, and green/turquoise glasses from Tebtynis are opacified using Ca, Na or a solid solution between Ca-Na or Ca-Na-Pb antimonates, where Pb substitution occurs only in soda-lime-lead or leaded glasses. Archaeometric analyses have demonstrated that Ca antimonates can be present in ancient glasses in two main synthetic phases (Lahlil et al., 2008; Shortland, 2008): orthorhombic ($Ca_2Sb_2O_7$) and hexagonal ($CaSb_2O_6$). The WDS and μ-Raman analyses performed on a selection of antimonate crystals in the opaque white, blue, and turquoise glasses from Tebtynis showed that both forms are present in all color classes, sometimes even within the same sample. This has been observed various times in the literature and during experimental melts, since the hexagonal phase tends to develop at the expense of the orthorhombic one with increasing times/temperatures during heat treatment (Lahlil, Biron, Cotte, & Susini, 2010). In particular, the hexagonal modification starts to form at 927°C and becomes the major phase at 1094°C (Lahlil et al., 2008).

One white (S-BiR-507-Bi), one turquoise (M-V-006a), and one dark blue (S-GB-413-B) sample from Tebtynis are mainly opacified with euhedral crystals of synthetic brizziite ($NaSbO_3$), while one light blue glass (M-A-005) shows a mixture of brizziite and romeite (Ca, Mn, Fe, $Na)_2(Sb, Ti)_2O_6(OH, F, O)$, as confirmed by WDS data and μ-Raman spectra. From bibliographic research, limited occurrences of brizziite have been identified to date in samples dated to the 1st millennium BCE or the early 1st millennium CE (de Ferri et al., 2020; Muros & Zacharias, 2019; Silvestri et al., 2015; and references therein). In one Roman case, the low amount of CaO (~2%) was used to tentatively explain the precipitation of brizziite, rather than the classic Ca antimonates. This is indeed true for the turquoise glass from Tebtynis, which is characterized by CaO of the order of 2%. However, the two other samples which contain brizziite show sufficient or even high concentrations of CaO (3.37% in the blue glass; 6.23% in the white glass); hence a different explanation is needed. Experimental synthesis of $NaSbO_3$ with ilmenite-type structure (Ramírez-Meneses et al., 2007) has demonstrated that under specific conditions this phase can precipitate at temperatures in the range of ~700–900°C, that are lower than those needed for Ca antimonates. It may therefore be argued that the samples containing brizziite were fired at lower temperatures, without reaching the thermal conditions for the precipitation of calcium antimonates. Further experimental data on the in situ crystallization of brizziite in ancient glasses are, however, strongly required to clarify the matter.

The Raman spectrum of romeite was also frequently identified in the opaque glasses from Tebtynis. Romeite is a cubic natural mineral, belonging to the pyrochlore supergroup (Atencio et al., 2010; Brugger et al., 1997). Considering its chemical similarity to the classic Ca antimonates and the fact that it is usually a minor phase with concentration < 1%, romeite was only identified in ancient glasses during a study on Roman mosaic *tesserae* of the 2nd century CE

performed using μ-Raman spectroscopy (Basso et al., 2014), since other analytical techniques such as XRD or SEM-EDS may not be sufficient for its specific characterization.

Euhedral romeite was found in one single sample of white glass (crystal size ~2–3 μm), while in all other cases euhedral crystals have spectra that can be attributed either to brizziite, $Ca_2Sb_2O_7$, or $CaSb_2O_6$. Conversely, anhedral aggregates (both compact and "rosary"-shaped) often show a mix of these various phases, as demonstrated by the frequent association of the peak at 512–514 cm^{-1} typical of romeite to the classic spectra of brizziite, $Ca_2Sb_2O_7$, or $CaSb_2O_6$. The romeite identified in the ancient glass samples cannot be attributed to a deliberate addition of the natural mineral to the base glass. Considering the shape, size, and chemical variability of the inclusions (as emerged from EDS data), it should be considered a synthetic phase just as the other, better-known, Ca antimonates.

Looking at the SEM-BSE images of the Ca-Na antimonate-opacified samples, four main types of texture can be recognized (Figure 7):

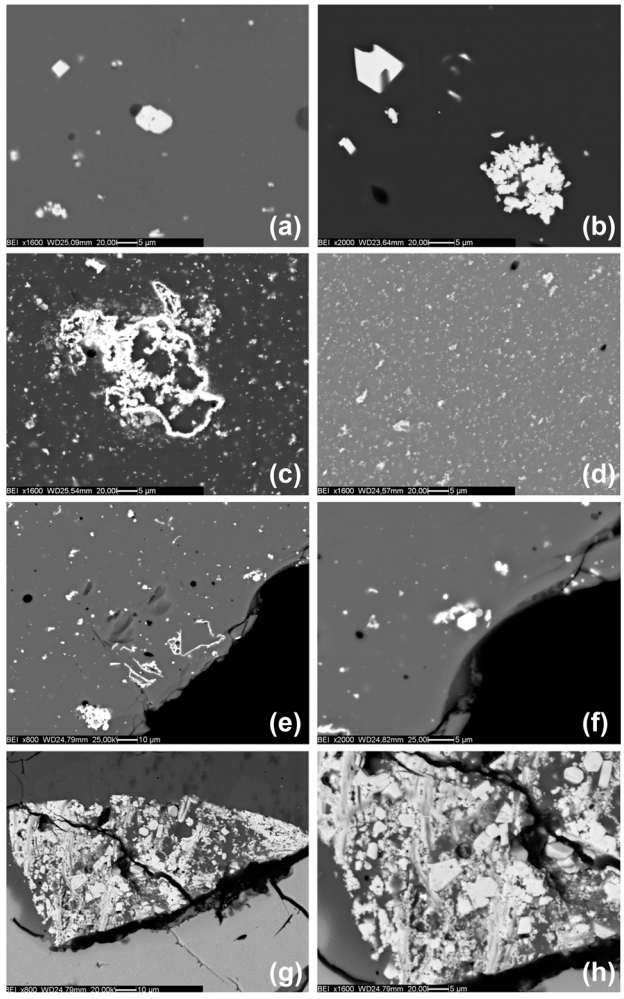

FIGURE 7 SEM-BSE images of the four types of textures identified in the opaque white, blue, and green glasses from Tebtynis: (a,b) texture (I) with small, euhedral crystals (I-B-616 and M-BAu-002); (c,d) texture (II) with "rosary"-shaped inclusions and flour-like effect (P-A-418 and M-V-005); (e,f) mixed texture (III) with both "rosary"-shaped aggregates and euhedral crystals in M-A-005, general view, and detail; (g,h) texture (IV) with angular lump with euhedral crystalline inclusions dispersed in a heterogeneous matrix, sample P-V-423-B, general view, and detail

- Texture (I) is characterized by the presence of small euhedral crystals (hexagonal or rectangular) with dimensions of 5 μm or less homogeneously, but not densely dispersed into the glass phase and often crystallized in small groups around the bubbles (Figure 7a,b).
- Texture (II) shows anhedral inclusions with "feathery" and "rosary" shapes, lacking any evidence of crystal faces or preferential growth directions. Their size varies widely: bigger aggregates can reach up to 100 μm and often display reacted edges partially dissolved into the glassy matrix; however, the majority of the crystals are sub-micrometric with a dense distribution, which produces a sort of flour-like effect in the glassy matrix (Figure 7c,d).
- Texture (III) exhibits a hybrid microstructure that combines "rosary"-shaped aggregates and rare euhedral crystals of micrometric size, alone or in small, segregated groups. In texture (III), "feathery" and "rosary"-shaped inclusions sometimes show preferential growth directions, with angles typical of the hexagonal system (Figure 7e,f).
- Texture (IV) was distinguished by the presence of a limited number of isolated, angular lumps with dimensions ranging from 70 to 100 μm, showing euhedral crystalline inclusions dispersed in a heterogeneous matrix (Figure 7g,h).

Textures (II) and (III) are especially found in white, light blue, and turquoise samples, while dark blue glasses can be mainly attributed to the texture (I) and, in minor measure, (III). Texture (IV) was only identified in one dark blue sample.

These micro-textural differences reflect the use of various production technologies for the opacification of glass. Hence the presence of small crystallites showing well-defined euhedral morphologies, with a medium to low number of crystals per unit area typical of texture (I) implies *in situ* crystallization. It has been suggested that antimony was intentionally added to the melt in the form of stibnite (Sb_2S_3) or oxides produced by roasting stibnite—that is, Sb_2O_3, Sb_2O_5 (Bimson & Freestone, 1983; Mass et al., 1998)—triggering the precipitation of calcium antimonate crystals and subtracting lime from the glass phase. However, the mean CaO contents in transparent (5.28%) and opaque (5.40%) dark blue glasses characterized by texture (I), are rather similar, possibly suggesting that to produce the Tebtynis dark blue glasses an extra supply of CaO was contextually provided.

Regarding the coloring techniques employed for opaque dark blue glasses from our set, the lower values of Sb_2O_5 and the double contents of FeO and TiO_2 with respect to the opaque white samples indicate that Co and Cu were not added to a white glass for coloring purposes. Similarly, the opaque dark blue glasses from Tebtynis are not the result of a mix between opaque white and transparent dark blue glass, as opaque dark blue samples contain, on average, higher CuO and CoO if compared to their transparent counterparts, thus implying that they were not diluted with white opaque glass. In synthesis, opaque dark blue glasses seem to be produced as an autonomous color class, with a specific recipe that did not imply the mixing of different batches.

The sub-micrometric, widespread crystals, sometimes aggregated in "rosary"- and "feathery"-shaped inclusions typical of texture (II), seem more consistent with the *ex situ* opacification process with calcium antimonate nano-crystals that was proposed by Lahlil, Biron, Cotte, Susini, and Menguy (2010) for LBA Egyptian glasses. This process implies the preliminary synthetization of Ca antimonate nano-crystals, which are subsequently added to a transparent glass batch. Since $Ca_2Sb_2O_7$ progressively transforms into $CaSb_2O_6$ with higher temperatures/longer firing times, it was proven that in the case of an *in situ* nucleation, when $Ca_2Sb_2O_7$ is the major phase, crystals cannot be of nanometric size. In our samples, nano-crystals of $Ca_2Sb_2O_7$ were observed in various white and turquoise samples through μ-Raman examination, suggesting that these glasses were probably produced with an *ex situ* process. However, a paper by Duckworth et al. (2012) has questioned this assumption after analyzing two "rosary"-shaped inclusions in two different samples of LBA turquoise and white glass, respectively. Time-of-flight secondary ion mass spectrometry showed that the average composition of the micro-

crystals was similar to that of the glassy matrix, suggesting direct precipitation from the melt. The problem should thus remain open until conclusive experimental data are presented.

Mixed texture (III) shows clear evidence of *in situ* nucleation, considering the presence of both directions of preferential growth for the "rosary"-shaped inclusions and euhedral crystals. However, at the moment it is not possible to determine if it is a primary crystallization directly from the glassy matrix or if the precipitation of the Ca-Na antimonates is secondary and due to the presence of intentionally added opacifiers, partially dissolved and recrystallized into the glass phase.

Finally, texture (IV) can be attributed to the voluntary *ex situ* addition of lumps of crushed, pre-fritted opacifiers incorporated into the glassy matrix at relatively low temperatures. This evidence bears a certain similarity to the *corpo* process used to produce modern mosaic *tesserae* in Venice (Lahlil et al., 2008). In this case, a vitreous phase very rich in *in situ* precipitated Ca antimonates is synthesized independently, ground, and added to a transparent glass of the desired color. The quantity of the *corpo*, its size, and distribution can be used to calibrate the opacity in the glass.

Summing up, the Tebtynis samples show that both *in situ* and *ex situ* techniques were in use at the same time in Ptolemaic Egypt and that general preferences for one process or the other can be broadly (but not systematically) seen between the different opaque color classes.

Looking at the white samples from Tebtynis in the context of earlier (LBA) and Graeco-Roman glasses from Egypt (Figure 8a), it is possible to distinguish the various chronological productions based on the alkali source. Moreover, it is interesting to note that no LBA glass is associated with the intermediate Mg-rich composition identified in five of the Tebtynis samples, while an *udjat*-eye mosaic plaque dated between the 3rd and the 1st century BCE (Goldstein, 1979) shows the exact same recipe (Brill, 1999; Brill & Moll, 1963), thus evidencing that this compositional signature can be considered as a marker of a group of Ptolemaic glasses. The presence of Mg-rich white glasses has also been noted by Nenna and Gratuze (2009), who found this peculiar composition in several of their Hellenistic samples discovered in various sites in Europe and Africa (Avenches and Augst in Switzerland and Heis in Somaliland) and in some unprovenanced samples from the Gorga collection. Unfortunately, the paper does not report the compositional values of each sample, so it was not possible to plot them as a reference.

Ionic colorants in blue glasses

The color of all blue glasses from Tebtynis is due to ionic colorants (see Supporting Information, Figure S3)—that is, copper (in light blue samples), cobalt, or a combination of cobalt and copper (in transparent and opaque dark blue samples, with CuO always ≤0.72%).

Copper is the earliest and most common chromophore used for vitreous materials (Tite, 1987). Starting from the LBA, traces of tin appear in Cu-colored glazes of faience objects (Kaczmarczyk & Hedges, 1983) sometimes with Cu:Sn ratios close to 10:1 by weight, suggesting that bronze started to be employed as copper-bearing raw material, in parallel with mineral sources.

Considering the Tebtynis samples, tin is essentially absent or very low (≤0.05%) in opaque and transparent dark blue glasses, while it is always present in the light blue glasses (Sn from 0.07% to 0.19%). The Cu:Sn ratio by weight shows a linear correlation in all light blue samples and a few opaque dark blue glasses, ranging between 13:1 and 28:1. The lowest values are compatible with a low-Sn bronze alloy (Odgen, 2000), while in most cases, if scrap bronze was used, some extra copper must have been (intentionally or unintentionally) supplied from other sources. This hypothesis is strengthened by the identification of a huge copper chip (~40 μm) in one of the opaque dark blue samples from Tebtynis (P-A-408-B; EDS data: Cu 98.5 wt%, Sn

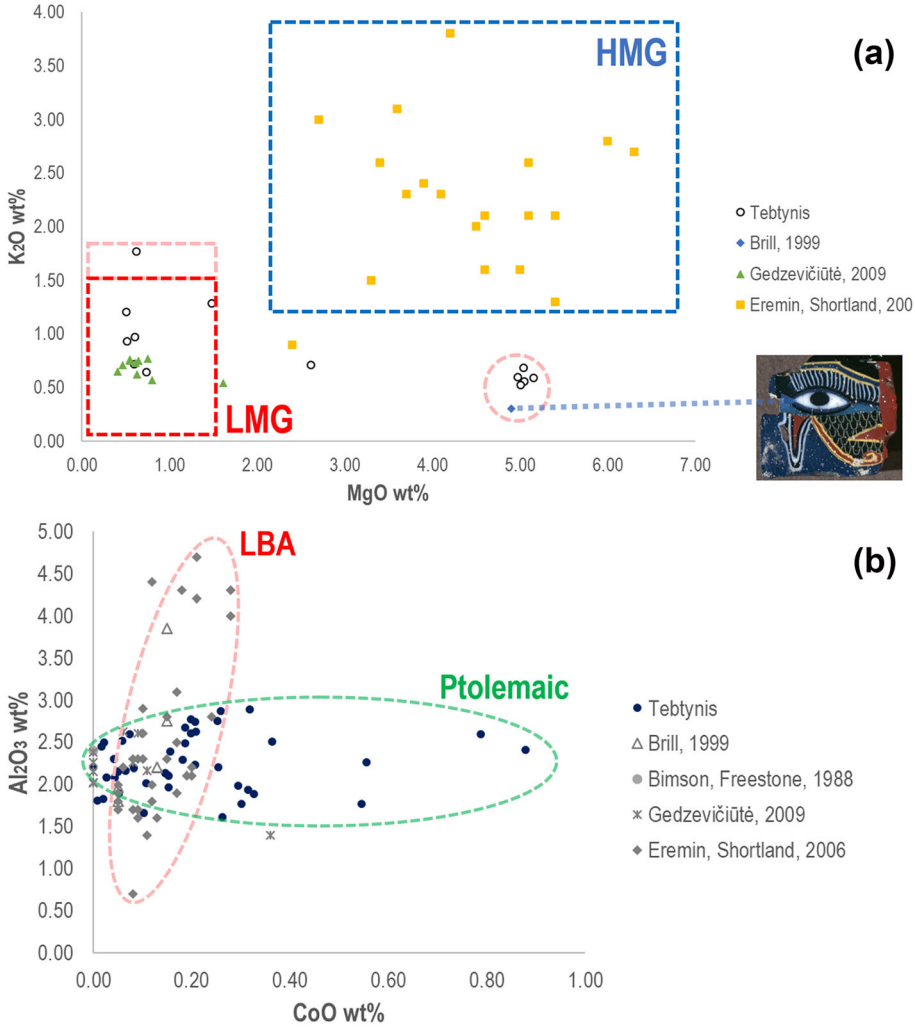

FIGURE 8 (a) K_2O versus MgO content of the glass phase in the Tebtynis white glasses (symbol: white dots) compared with a series of LBA white glasses published by Shortland and Eremin (2006) (symbol: yellow squares) and with coeval glasses analyzed by Brill (1999) (blue diamonds) and Gedzevičiūtė et al. (2009) (symbol: green triangles). Compositional classes from Henderson (2013) are defined by dotted lines. (b) Al_2O_3 versus CoO content in the glass phase of the blue samples from Tebtynis (dark blue dots) and other earlier and coeval sites considered in the literature; specifically: LBA glasses from Shortland and Eremin (2006) (gray diamonds), and late period and Ptolemaic glasses published by Brill (1999) (gray triangles), Bimson and Freestone (1988) (gray dots) and Gedzevičiūtė et al. (2009) (gray asterisks). Chronological trends are defined by dotted lines

0.3 wt%), which suggests that—at least in certain cases—pure copper was added as an independent coloring agent.

Cobalt is the strongest coloring agent used in antiquity, as it can impart a distinct blue color to the glass in concentrations of 0.02 wt% or even lower. However, noteworthy levels of copper have been reported in various Co-colored glasses over a wide chronological period, which led to the hypothesis of a voluntary addition aimed to enhance the final color (Walton et al., 2012).

According to Kaczmarczyk and Hedges (1983), during the Late Period and especially throughout the Ptolemaic and Roman eras, Egyptian Co-colored faience glazes exhibit significantly lower values of MnO than in the previous phases. The authors associate this

compositional change with a technological shift from the exploitation of the cobaltiferous ores of the Western desert to the discovery of different mines of Mn-free, Co-bearing sulfides, and arsenides, which were tentatively suggested to be located in Iran. Among the analyzed dark blue samples from Tebtynis, there is no evident correlation between CoO and Al_2O_3 and neither between CoO and MgO or Sb_2O_5 (for Sb_2O_5 only transparent samples were considered). There is, however, a discrete correlation between CoO and MnO in a group of dark blue glasses (mainly transparent), suggesting that the two elements might derive from the same source. Unfortunately, due to the detection limits of EPMA, the contents of NiO and ZnO of the Tebtynis glasses cannot be used for exploring the issue of CoO provenance; further investigations by LA-ICP-MS are planned to clarify the matter. Currently, there is no chance to propose a specific origin for the cobaltiferous ore used. What can be said with high confidence is that the ratio MnO/CoO is very different from that of the coeval manganese-free faience glazes; this seems to suggest that minerals of the asbolane group might have been used as the cobalt source.

Another possible explanation for the correlating values of cobalt and manganese can be ascribed to the (de)coloring properties of this element. In fact, in a Venetian recipe book of the 16th century CE it is explicitly noted that when the blue glass has a purple tint the color gets deeper and shinier (Seccaroni & Haldi, 2016). One transparent dark blue sample from Tebtynis has peculiar zoning consisting of bands with varying amounts of CuO, CoO, and MnO, anti-correlated with the FeO values, which is the result of the uneven mixing of the coloring agents into the glassy matrix (Figure 5a). This further proves the association between CoO, CuO, and MnO (and the lack of a direct relation with Al_2O_3, As_2O_5, Sb_2O_5, and PbO), but again it does not give specific hints about the raw materials used.

Considering the Tebtynis (Cu)Co-colored samples in a diachronic perspective, the difference from LBA productions becomes apparent. The Al_2O_3 versus CoO plot highlights two well-defined compositional trends (Figure 8b): whereas in LBA glasses Al_2O_3 drastically increases with increasing CoO content, during the Ptolemaic period, alumina is independent from cobalt and ranges in the variability of the sand source, as shown by the analyzed specimen and other coeval samples. Moreover, the average amount of cobalt per sample seems to rise significantly moving towards the Roman period, which can perhaps be linked with the wider availability of the raw material.

Opaque turquoise glasses

Looking at the PCA (see Supporting Information, Figure S4), turquoise glasses exhibit a good compositional consistency, having high Sb_2O_5, low FeO (0.19–0.87%), and moderate to high amounts of copper (CuO 1.58–5.48%), that reflect the recipe of Cu-colored and antimonate-opacified LMG glasses. Transparent green samples are clustered in two groups, indicating that they were produced using different raw materials: three samples are characterized by high levels of CaO, K_2O, MgO, and FeO, which are consistent with plant ash glass colored by a mixture of Fe^{2+} and Fe^{3+} ions (CuO is very low, from 0.02% to 0.3%, not sufficient for coloring). Conversely, two samples have significant concentrations of PbO, CuO, Al_2O_3, and SnO_2, and can be interpreted as leaded-LMG glasses colored with copper (CuO 4.85 wt% and 5.35 wt%) and iron (FeO 1.48–1.79 wt%).

As already noted, turquoise glasses are opacified through Ca antimonate inclusions, often characterized by anhedral habit and minor substitutions of Ca with Na and, more frequently, low amounts of Pb (when present, it usually accounts for 2–4 wt%). This is consistent with what is reported in the literature on Ptolemaic (Bimson & Freestone, 1988) and Roman glass (Basso et al., 2014; Gedzevičiūtė et al., 2009; Silvestri et al., 2014), even if examples of Pb antimonate (Basso et al., 2014; Gliozzo et al., 2010) or cassiterite-opacified (Gedzevičiūtė et al., 2009) green

glasses were also reported, but mainly dated to the Late Antiquity. Lead antimonate, in association with copper, is also known as the main colorant/opacifier in the few analyzed LBA opaque green glasses from Egypt (Shortland & Eremin, 2006), but has not been identified in the Tebtynis samples analyzed during this work.

The number of published archaeometric analyses related to pre-Roman opaque greens is very scarce. Nevertheless, the difference between the two chronological phases is very neat: New Kingdom glasses have low levels of both antimony and lead, despite being colored with a combination of copper and Pb antimonates. Conversely, Ptolemaic glasses have Sb_2O_5 always over 1 wt% and variable amounts of lead, from absent to very high (sometimes over 10 wt%), which evidences the presence of two subgroups: one comprising high-Pb and the other low-Pb LMG turquoise glasses. All the Graeco-Roman samples considered (including those from the literature) were opacified using Ca antimonates, with minor substitutions of Ca with Na and Pb (only in leaded glasses).

More analyses are still needed to better contextualize this heterogeneous class, but considering the Tebtynis glasses as a representative sample of Ptolemaic glass production it is finally possible to address the question posed by Bimson and Freestone back in 1988 (Bimson & Freestone, 1988). The green ingot emerged from the foundation depot of the Osiris temple in Canopus (British Museum, Department of Greek and Roman Antiquities, inv. 1895 10-30 3) and dedicated by Ptolemy III and Queen Berenice around 246–221 BCE is surely not an aberrant red and, indeed, it can be included in the composite class of opaque green Ptolemaic glasses.

CONCLUSIONS

The artifacts from the Tebtynis workshop carry important information about the technologies of production and manufacturing processes used under Ptolemaic rule, offering a preliminary insight into the complexity of the Egyptian glass industry.

The multi-methodological analysis performed during this research highlighted the coexistence of glasses produced using two different alkali sources: the classic LMG composition is predominant, but a few samples confirm the use of plant-ash (HMG) at least in colorless, transparent blue, and transparent green glasses. Moreover, the Tebtynis samples show interesting comparisons for specific compositional groups which were considered anomalous, such as the high-Mg white glasses or the green ingot analyzed by Bimson and Freestone (1988).

From the compositional point of view, the samples from Tebtynis are well integrated into the evolutionary trajectory leading to Roman glass. Looking at the coloring techniques, the site stands at the edge between two worlds, with ancient recipes coexisting with newer ones. This is clearly shown by the combined use of *ex situ* and *in situ* precipitation of Ca antimonates, where the first approach is especially typical of LBA Egyptian glasses, while the second seems to prevail in the Roman production. Also, we discovered explicit evidence in the microstructure of the glass for the use of the *corpo* technique in the Hellenistic period.

This work offers a huge compositional database derived from the investigation of a reasoned selection of the finished and semi-finished glasses from Tebtynis, an exceptionally well-preserved Egyptian workshop, sealed by the functional transformation of the area at the beginning of the Roman rule. For this reason, the analytical data published in this paper can be considered as a reference assemblage for future works on Hellenistic and early Roman Egyptian glasses, offering a solid starting point for any research related to early Mediterranean glasses from the 1st millennium BCE to the 1st millennium CE.

ACKNOWLEDGEMENTS

The *Museo Egizio, Torino* and the *Soprintendenza Archeologia, Belle Arti e Paesaggio per la città metropolitana di Torino*, in particular Christian Greco, Alessia Fassone, and Matilde Borla, are heartfully thanked for favoring access to the materials and for sampling authorizations. Gianmario Molin and Paola Zanovello are also sincerely acknowledged for their support to the project. The Open Access fees were funded by the University of Padova. Open Access Funding provided by Universita degli Studi di Padova within the CRUI-CARE Agreement.

AUTHOR CONTRIBUTIONS

Conceptualization, methodology, sampling, validation, data interpretation: Cinzia Bettineschi and Ivana Angelini. *Software, formal analysis, investigation, data curation, visualization, and writing—original draft preparation*: Cinzia Bettineschi. *Writing—review and editing*: Cinzia Bettineschi and Ivana Angelini. *Supervision*: Ivana Angelini. Both authors have read and agreed to the published version of the manuscript.

DATA AVAILABILITY STATEMENT

The data that supports the findings of this study are available in the text and supplementary material of this article.

ORCID

Cinzia Bettineschi https://orcid.org/0000-0001-5322-4815
Ivana Angelini https://orcid.org/0000-0002-7970-3416

REFERENCES

Aerts, A., Velde, B., Janssens, K., & Dijkman, W. (2003). Change in silica sources in Roman and post-Roman glass. *Spectrochimica Acta - Part B Atomic Spectroscopy*, *58*(4), 659–667. https://doi.org/10.1016/S0584-8547(02)00287-2

Angelini, I., Gratuze, B., & Artioli, G. (2019). Glass and other vitreous materials through history. *European Mineralogical Union Notes in Mineralogy*, *20*, 87–150. https://doi.org/10.1180/EMU-notes.20.3

Atencio, D., Andrade, M. B., Christy, A. G., Giere, R., & Kartashov, P. M. (2010). The Pyrochlore Supergroup of minerals: Nomenclature. *The Canadian Mineralogist*, *48*(3), 673–698. https://doi.org/10.3749/canmin.48.3.673

Barkoudah, Y., & Henderson, J. (2006). Plant ashes from Syria and the manufacture of ancient glass: Ethnographic and scientific aspects. *Journal of Glass Studies*, *48*, 297–321.

Basso, E., Invernizzi, C., Malagodi, M., La Russa, M. F., Bersani, D., & Lottici, P. P. (2014). Characterization of colorants and opacifiers in roman glass mosaic tesserae through spectroscopic and spectrometric techniques. *Journal of Raman Spectroscopy*, *45*(3), 238–245. https://doi.org/10.1002/jrs.4449

Bettineschi, C., Angelini, I., & Molin, G. (2019). Contestualizzazione degli intarsi in vetro da Tebtynis nel quadro dell'Egitto Greco-Romano. In I. Favaretto, F. Ghedini, P. Zanovello, & E. M. Ciampini (Eds.), *Anti. Archeologia. Archivi* (pp. 515–540). IVSLA Edizioni.

Bettineschi, C., Deotto, G., Begg, D. J. I., Molin, G., Zanovello, P., Fassone, A., Greco, C., Borla, M., & Angelini, I. (2019). A dig through archives and depots: Rediscovering the inlay workshop of Tebtynis and its materials. *Nuncius*, *34*(3), 485–516. https://doi.org/10.1163/18253911-03403001

Bimson, M., & Freestone, I. C. (1983). An analytical study of the relationship between the Portland vase and other Roman cameo glasses. *Journal of Glass Studies*, *25*, 55–65.

Bimson, M., & Freestone, I. C. (1988). Some Egyptian glasses dated by Royal Inscriptions. *Journal of Glass Studies*, *30*, 11–15.

Brill, R. H. (1999). Chemical analysis of early glasses. Volume 2: Tables of Analyses, **Volume 2**, 335.

Brill, R. H., & Moll, S. (1963). The Electron Beam Probe in the Microanalysis of Ancient Glass. In *Advances in glass technology, part 2* (Vol. 6, pp. 239–302). Plenum Press.

Brugger, J., Gieré, R., Graeser, S., & Meisser, N. (1997). The crystal chemistry of roméite. *Contributions to Mineralogy and Petrology*, *127*(1–2), 136–146. https://doi.org/10.1007/s004100050271

de Ferri, L., Mezzadri, F., Falcone, R., Quagliani, V., Milazzo, F., & Pojana, G. (2020). A non-destructive approach for the characterization of glass artifacts: The case of glass beads from the iron age Picene necropolises of Novilara and Crocefisso-Matelica (Italy). *Journal of Archaeological Science: Reports*, *29*, 102124. https://doi.org/10.1016/j.jasrep.2019.102124

Deer, W. A., Howie, R. A., & Zussman, J. (2013). *An introduction to the rock-forming minerals*. Mineralogical Society of Great Britain and Ireland.

Degryse, P. (2014). *Glass making in the Greco-Roman world: Results of the ARCHGLASS project*. Leuven University Press. https://doi.org/10.26530/OAPEN_513796

Degryse, P., Henderson, J., & Hodgins, G. (Eds.) (2009). *Isotopes in vitreous materials*. Leuven University Press.

Duckworth, C. N., Henderson, J., Rutten, F. J. M., & Nikita, K. (2012). Opacifiers in late bronze age glasses: The use of ToF-SIMS to identify raw ingredients and production techniques. *Journal of Archaeological Science*, *39*(7), 2143–2152. https://doi.org/10.1016/j.jas.2012.02.011

El-Hinnawi, E. E. (1964). Mineralogical and geochemical studies on Egyptian (U.a.R.) black sands. *Beitrage Zur Mineralogie Und Petrographie*, *9*(6), 519–532. https://doi.org/10.1007/BF01104489

Fiori, C. (2015). Production technology of byzantine red mosaic glasses. *Ceramics International*, *41*(2), 3152–3157. https://doi.org/10.1016/j.ceramint.2014.10.160

Foster, H. E., & Jackson, C. M. (2009). The composition of "naturally coloured" late Roman vessel glass from Britain and the implications for models of glass production and supply. *Journal of Archaeological Science*, *36*(2), 189–204. https://doi.org/10.1016/j.jas.2008.08.008

Gedzevičiūtė, V., Welter, N., Schüssler, U., & Weiss, C. (2009). Chemical composition and colouring agents of Roman mosaic and millefiori glass, studied by electron microprobe analysis and Raman microspectroscopy. *Archaeological and Anthropological Sciences*, *1*, 15–29. https://doi.org/10.1007/s12520-009-0005-4

Gliozzo, E. (2017). The composition of colourless glass: A review. *Archaeological and Anthropological Sciences*, *9*(4), 455–483. https://doi.org/10.1007/s12520-016-0388-y

Gliozzo, E., Santagostino Barbone, A., D'acapito, F., Turchiano, M., Turbanti Memmi, I., & Volpe, G. (2010). The Sectilia panels of faragola (Ascoli Satriano, southern Italy): A multi-analytical study of the green, marbled (green and yellow), blue and blackish glass slabs. *Archaeometry*, *52*(3), 389–415. https://doi.org/10.1111/j.1475-4754.2009.00493.x

Goldstein, S. M. (1979). *Pre-Roman and early Roman glass in the corning Museum of Glass*. The Corning Museum of Glass.

Grose, D. F. (1989). *Early ancient glass*. Hudson Hills Press.

Henderson, J. (1985). The raw materials of early glass production. *Oxford Journal of Archaeology*, *4*(3), 267–291. https://doi.org/10.1111/j.1468-0092.1985.tb00248.x

Henderson, J. (1988). Glass production and bronze age Europe. *Antiquity*, *62*(236), 435–451. https://doi.org/10.1017/S0003598X00074548

Henderson, J. (2000). *The science and archaeology of materials: An investigation of inorganic materials*. Routledge.

Henderson, J. (2013). *Ancient glass: An interdisciplinary exploration*. Cambridge university Press. https://doi.org/10.1017/CBO9781139021883

Hilmy, M. E. (1951). Beach Sands of the Mediterranean coast of Egypt. *SEPM Journal of Sedimentary Research*, *21*, 109–120. https://doi.org/10.1306/D4269436-2B26-11D7-8648000102C1865D

Jackson, C. M., Paynter, S., Nenna, M. D., & Degryse, P. (2018). *Glassmaking using natron from el-Barnugi (Egypt); Pliny and the Roman glass industry*. Archaeological and Anthropological Sciences.

Kaczmarczyk, A., & Hedges, R. E. M. (1983). *Ancient Egyptian faience: An analytical survey of Egyptian faience from Predynastic to Roman times*. Aris and Phillips.

Lahlil, S., Biron, I., Cotte, M., & Susini, J. (2010). New insight on the in situ crystallization of calcium antimonate opacified glass during the Roman period. *Applied Physics a: Materials Science and Processing*, *100*(3), 683–692. https://doi.org/10.1007/s00339-010-5650-z

Lahlil, S., Biron, I., Cotte, M., Susini, J., & Menguy, N. (2010). Synthesis of calcium antimonate nano-crystals by the 18th dynasty Egyptian glassmakers. *Applied Physics a: Materials Science and Processing*, *98*, 1–8. https://doi.org/10.1007/s00339-009-5454-1

Lahlil, S., Biron, I., Galoisy, L., & Morin, G. (2008). Rediscovering ancient glass technologies through the examination of opacifier crystals. *Applied Physics a: Materials Science and Processing*, *92*(1), 109–116. https://doi.org/10.1007/s00339-008-4456-8

Larson, K. A. (2016). *From luxury product to Mass commodity: Glass production and consumption in the Hellenistic world*. University of Michigan.

Lucas, A., & Harris, J. R. (1962). *Ancient Egyptian materials and industries* (IV ed.). Edward Arnold Publishers.

Mass, J. L., Stone, R. E., & Wypyski, M. T. (1998). The mineralogical and metallurgical origins of Roman opaque colored glasses. In P. McCray & W. D. Kingery (Eds.), *The prehistory and history of glassmaking technology* (pp. 251–268). The American Ceramics Society.

Mass, J. L., Wypyski, M. T., & Stone, R. E. (2002). Malkata and Lisht glassmaking technologies: Towards a specific link between second millennium BC metallurgists and glassmakers. *Archaeometry*, *44*(1), 67–82. https://doi.org/10.1111/1475-4754.00043

Muros, V., & Zacharias, N. (2019). Lines, spots and trails: A microscopic and mineralogical study of antimonate-opacified glass beads from Lofkënd, Albania. *Archaeological and Anthropological Sciences*, *11*(5), 1769–1782. https://doi.org/10.1007/s12520-018-0627-5

Nenna, M. D. (2015). Primary Glass Workshops in Graeco-Roman Egypt: Preliminary Report on the Excavations of the Site of Beni Salama Wadi Natrun (2003, 2005–9). In *Glass of the Roman world* (pp. 1–22). Oxbow Books.

Nenna, M.-D., & Gratuze, B. (2009). Étude Diachronique des Compositions de Verres Employés dans les vases mosaiqués antiques: résultats préliminarires. In K. Janssens, P. Degryse, P. Cosyns, J. Caen, & L. Van't Dack (Eds.), *Annales du 17e Congrès de l'Association International pour l'Histoire du Verre, Anvers 2006* (pp. 199–205). University Press Antwerp.

Nenna, M. -D., Picon, M., & Vichy, M. (2000). Ateliers primaires et secondaires en Egypte à l'époque gréco-romaine. *La Route du verre. Ateliers primaires et secondaires du second millénaire av*. J.-C. au Moyen Âge.

Nicholson, P. T. (Ed.) (2007). *Brilliant things for Akhenaten. The production of glass, vitreous materials and pottery at Amarna site O45.1*. Egypt Exploration Society.

Odgen, J. (2000). Metals. In P. T. Nicholson & I. Shaw (Eds.), *Ancient Egyptian productions and technology* (pp. 148–176). Cambridge University Press.

Olmi, F., & Sabelli, C. (1994). Brizziite, NaSbO3, a new mineral from the Cetine mine (Tuscany, Italy): Description and crystal structure. *European Journal of Mineralogy*, *6*(5), 667–672. https://doi.org/10.1127/ejm/6/5/0667

Paynter, S., & Jackson, C. (2019). Clarity and brilliance: Antimony in colourless natron glass explored using Roman glass found in Britain. *Archaeological and Anthropological Sciences*, *11*(4), 1533–1551. https://doi.org/10.1007/s12520-017-0591-5

Push, E., & Rehren, T. (2007). *Hochtemperatur-Technologie in der Ramses-Stadt*. Rubinglas für den Pharao.

Ramírez-Meneses, E., Chavira, E., Domínguez-Crespo, M. A., Escamilla, R., Flores-Flores, J. O., & Soto-Guzmán, A. B. (2007). Synthesis and characterization of NaSbO3 compound. *Superficies Y Vacío*, *20*(4), 14–18.

Rapp, G. R. (2017). Archaeomineralogy.

Rehren, T., & Rosenow, D. (2020). Three Millennia of Egyptian Glassmaking. In *Mobile Technologies in the Ancient Sahara and beyond* (pp. 423–450). Cambridge University Press.

Rosenow, D., & Rehren, T. (2014). Herding cats - Roman to late antique glass groups from Bubastis, northern Egypt. *Journal of Archaeological Science*, *49*(1), 170–184. https://doi.org/10.1016/j.jas.2014.04.025

Sayre, E. W., & Smith, R. W. (1961). Compositional categories of ancient glass. *Science*, *133*(3467), 1824–1826. https://doi.org/10.1126/science.133.3467.1824

Schibille, N., Sterrett-Krause, A., & Freestone, I. C. (2017). Glass groups, glass supply and recycling in late Roman Carthage. *Archaeological and Anthropological Sciences*, *9*, 1223–1241. https://doi.org/10.1007/s12520-016-0316-1

Seccaroni, C., & Haldi, J.-P. (2016). *Cobalto, zaffera, smalto dall'antichità al XVIII secolo*. Enea.

Shortland, A. J. (2008). The use and origin of antimonate colorants in early Egyptian glass*. *Archaeometry*, *44*, 517–530. https://doi.org/10.1111/1475-4754.t01-1-00083

Shortland, A. J., & Eremin, K. (2006). The analysis of second millennium glass from Egypt and Mesopotamia, part 1: New WDS analysis. *Archaeometry*, *48*(4), 581–603. https://doi.org/10.1111/j.1475-4754.2006.00274.x

Silvestri, A., Molin, G., Salviulo, G., & Schievenin, R. (2006). Sand for Roman glass production: An experimental and philological study on source of supply. *Archaeometry*, *48*(3), 415–432. https://doi.org/10.1111/j.1475-4754.2006.00264.x

Silvestri, A., Tonietto, S., Molin, G., & Guerriero, P. (2014). The palaeo-Christian glass mosaic of St. Prosdocimus (Padova, Italy): Archaeometric characterisation of tesserae with copper- or tin-based opacifiers. *Journal of Archaeological Science*, *42*(1), 51–67. https://doi.org/10.1016/j.jas.2013.10.018

Silvestri, A., Tonietto, S., Molin, G., & Guerriero, P. (2015). Multi-methodological study of palaeo-Christian glass mosaic tesserae of St. Maria mater Domini (Vicenza, Italy). *European Journal of Mineralogy*, *27*(2), 225–245. https://doi.org/10.1127/ejm/2015/0027-2427

Stern, E. M. (2012). Glass production. In J. P. Oleson (Ed.), *The Oxford handbook of engineering and technology in the classical world*. Oxford Handbooks (pp. 520–548). Oxford University Press.

Stern, E. M., & Schlick-Nolte, B. (1994). *Early glass of the ancient world, 1600 B.C. to a.D. 50: Ernesto wolf collection*. Gerd Hatje.

Takla, M. A., & Arafa, E. H. (1975). The mineralogy of the sand dunes between Minya and Dairut, Egypt. *TMPM Tschermaks Mineralogische Und Petrographische Mitteilungen*, *22*(2), 164–173. https://doi.org/10.1007/BF01089115

Tite, M., Pradell, T., & Shortland, A. (2008). Discovery, production and use of tin-based opacifiers in glasses, enamels and glazes from the late iron age onwards: A reassessment. *Archaeometry*, *50*(1), 67–84.

Tite, M. S. (1987). Characterisation of early vitreous materials. *Archaeometry*, *29*(1), 21–34. https://doi.org/10.1111/j.1475-4754.1987.tb00394.x

Tite, M. S., Shortland, A. J., & Bouquillon, A. (2008). Glazed Steatite. In M. S. Tite & A. J. Shortland (Eds.), *Production Technology of Faience and Related Early Vitreous Materials* (pp. 23–36). Oxford University School of Archaeology.

Turner, W. E. S. (1956). Studies in ancient glasses and Grasmaking processes. Part V. Raw materials and melting processes. *Journal of the Society of Glass Technology*, *40*, 277–300.

Van Ham-Meert, A., Dillis, S., Blomme, A., Cahill, N., Claeys, P., Elsen, J., Eremin, K., Gerdes, A., Steuwe, C., Roeffaers, M., Shortland, A., & Degryse, P. (2019). A unique recipe for glass beads at iron age Sardis. *Journal of Archaeological Science*, *108*(June), 104974. https://doi.org/10.1016/j.jas.2019.104974

Walton, M., Eremin, K., Shortland, A., Degryse, P., & Kirk, S. (2012). Analysis of late bronze age glass axes from nippur-a new cobalt colourant. *Archaeometry*, *54*(5), 835–852. https://doi.org/10.1111/j.1475-4754.2012.00664.x

SUPPORTING INFORMATION

Additional supporting information can be found online in the Supporting Information section at the end of this article.

How to cite this article: Bettineschi, C., & Angelini, I. (2022). Reflections into Ptolemaic glass: Colorless, white, blue, and green inlays from the workshop of Tebtynis. *Archaeometry*, 1–38. https://doi.org/10.1111/arcm.12825